NASA Technical Paper 3406

1993

A Review of Recent Aeroelastic Analysis Methods for Propulsion at NASA Lewis Research Center

T.S.R. Reddy, Milind A. Bakhle, and R. Srivastava
University of Toledo
Toledo, Ohio

Oral Mehmed and George L. Stefko
Lewis Research Center
Cleveland, Ohio

NASA
National Aeronautics and Space Administration
Office of Management
Scientific and Technical Information Program

Summary

This report reviews aeroelastic analyses for propulsion components (propfans, compressors, and turbines) being developed and used at the NASA Lewis Research Center. These aeroelastic analyses include both structural and aerodynamic models. The structural models include a typical section, a beam (with and without disk flexibility), and a finite-element blade model (with plate bending elements). The aerodynamic models are based on the solution of equations ranging from the two-dimensional linear potential equation to the three-dimensional Euler equations for multibladed configurations. Typical calculated results are presented for each aeroelastic model. Suggestions for further research are made. Many of the currently available aeroelastic models and analysis methods are being incorporated in a unified computer program, APPLE (Aeroelasticity Program for Propulsion at LEwis).

Introduction

An historical perspective of the design and development of compressor systems for aircraft gas turbine engines, with emphasis on the current research at the NASA Lewis Research Center, is presented in reference 1. The author noted that further advances in the technology of aircraft turbomachinery systems would depend largely on the ability to more accurately model and properly account for the unsteady flows and their effects in the design process. He concluded that solving the problems associated with unsteady flow phenomena, such as the loss of stall margin with inlet distorted flows, blade flutter within the operating range, and premature blade failures due to forced-response excitations, have begun to consume more and more of the total development cost of new engine systems.

Turbine and compressor blade failures due to vibrations from unsteady flow can be traced to the infancy of the aircraft gas turbine (refs. 2 and 3). The vibrations leading to such failures can be stable, as in the case of forced vibrations from upstream flow distortions, or they can be unstable, as in the case of self-excited vibrations (flutter). In either case, the problems are aeroelastic in nature. Addressing these problems is important for the development and operation of advanced aircraft engines. Data relevant to aeroelastic instabilities (flutter) for several types of turbojet and turbofan engines are presented in reference 4. These data were obtained from a joint NASA/USAF Engine System Research program. A synthesis of these data showed that many types of flutter can occur near the operating line, triggered by different flow conditions (fig. 1(a)). The early reports of aeroelastic instability were presented for turbines and compressors; however, the newly developed advanced propellers (propfans) have also shown a susceptibility to aeroelastic instability (refs. 5 and 6). A rotor may also have forced-response excitations and fatigue failures from dynamic amplification and resonance, which occurs when an excitation frequency is near or at a blade natural frequency. A Campbell diagram for a rotor blade (fig.1(b)) can be used to identify possible resonant speeds at intersections of exciting and natural frequency lines.

Aeroelasticity is the science that deals with the mutual interaction between aerodynamic forces and elastic forces of a flexible structure, which in this case is a propulsion component: a propeller (propfan), compressor, or turbine. A correct understanding of aeroelastic characteristics is necessary to eliminate the problems just described. Aeroelastic analysis methods for wings, wing bodies, or complete aircraft (i.e., aeroelastic methods related to external flow) have now become fairly well established. Linear methods are available for computations if the flow is in either the subsonic or supersonic range. However, for complex flows containing shock waves, vortices, and flow separations, computational methods are needed (refs. 7 and 8). Aeroelastic research, in parallel with developments for wing and wing bodies, has been in progress to develop aeroelasticity methods for propulsion components (i.e., aeroelastic methods related to internal flow). A review of this progress is presented in references 9 to 11.

For the last several years, NASA Lewis Research Center has been developing aeroelastic analyses for turbomachines and propfans. This work has resulted in individual codes with differences in the aerodynamic and structural models used. However, a single consolidated computer program does not exist for effective use by designers and researchers. The availability of numerous computers from desktop workstations to supercomputers and the development of both graphical user interfaces and concurrent engineering principles will allow consolidation of all related computer codes and aeroelastic analysis methods in a single computing system that provides common input and output data bases. Such a system, called APPLE (Aeroelasticity Program for Propulsion at LEwis), is under development. It is the authors' belief that such a system will complement the Numerical

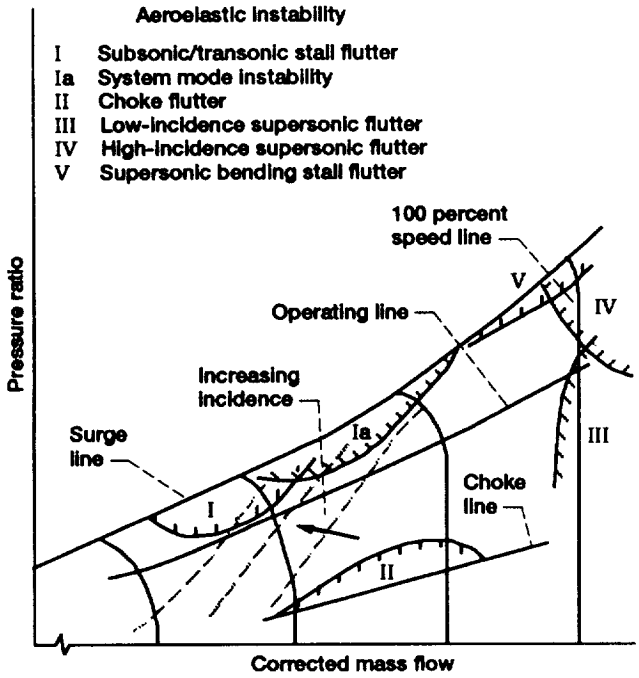

(a) Map showing principal types of flutter and regions of occurrence (ref. 4).

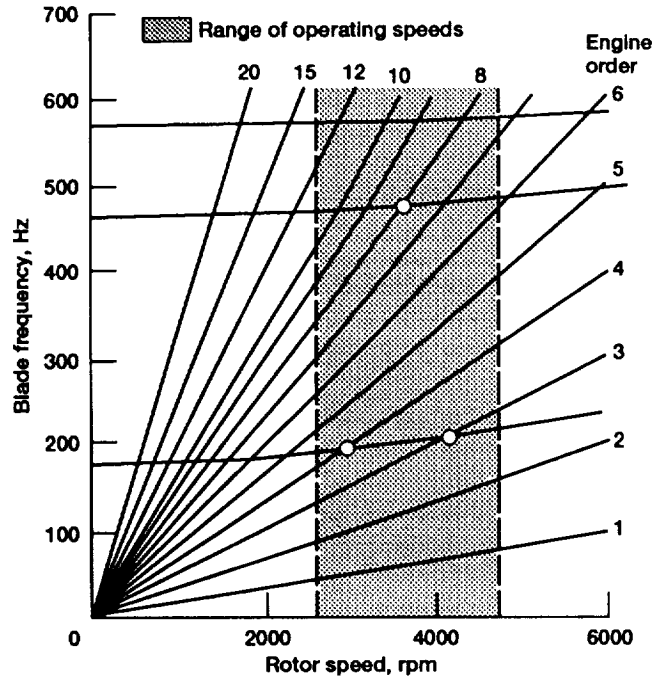

(b) Campbell diagram for rotor blade showing possible forced-response condition from resonance (denoted by circles).

Figure 1.—Aeroelastic stability boundaries and forced-response conditions for turbomachines and fans.

Propulsion Systems Simulator (NPSS), also under development at NASA Lewis (ref. 12).

This paper reviews the different aeroelastic analysis methods developed and implemented at NASA Lewis since 1978 (some of which are documented in ref. 13) for turbomachines and propfans. The aerodynamic models vary from those based on the linear potential equation to those based on nonlinear full potential and Euler equations. For aeroelastic analysis, the aerodynamic models were combined with structural models that included the typical section, beam (with and without disk flexibility), and finite-element blade model. Table I summarizes the aerodynamic models (now incorporated in APPLE) and their aeroelastic applications.

Note that the majority of the results presented herein are for propfan configurations because they were the primary focus of research from 1980 to 1990. However, the analysis methods are general and can predict blade flutter and forced-response excitations for turbomachines as well.

This paper is dedicated to the memory of Dr. Krishna Rao V. Kaza, who introduced the authors to the field of turbomachinery aeroelasticity.

Multibladed Structures Versus Fixed-Wing Aircraft

For aeroelastic analysis, the blades of a compressor, turbine, or propfan (as shown in fig. 2(a)) are represented as a cascade of blades rather than as isolated blades. A two-dimensional cascade representation of such a multibladed structure is obtained by unwrapping blade sections along a stream surface (fig. 2(b)). Phenomena that are not encountered with fixed wing surfaces can be attributed to the distinctive features of multibladed rotating structures: both aerodynamic and structural coupling result from the large multiplicity of closely spaced and mutually interfering blades; blade attachment and disk flexibility may vary greatly; the effect of centrifugal loading is present. Another distinctive feature of multibladed structures is that the nature of the cascade flow depends on the inlet Mach number and the stagger angle; for supersonic flow, the axial component of the flow may be subsonic or supersonic, giving rise to different Mach reflection patterns (fig. 3). In addition, two other features distinguish the multibladed fluid-structure interaction problems from fixed-wing or isolated airfoil problems: (1) structural mistuning and (2) aerodynamic mistuning. Structural mistuning refers to slight differences in structural properties between the blades of a turbomachine or propfan. This mistuning can cause localized mode vibrations in which all the energy in the system is concentrated in one or two blades, leading to blade failure or loss. Aerodynamic mistuning refers to differences in blade-to-blade spacing and pitch angles. This mistuning alters the unsteady flow characteristics in the blade passage. In the present report, only

TABLE I.—SUMMARY OF AERODYNAMIC MODELS AND THEIR AEROELASTIC APPLICATIONS

Aerodynamic model		Author	Reference	Equation type	Aeroelastic application	Reference
Model type[a]	Flow					
I	Incompressible	Whitehead, 1960	30	2-D	Kaza and Kielb, 1982	18
I	Subsonic	Smith, 1973	31	2-D	Kielb and Kaza, 1983	46
		Rao and Jones, 1975	32	2-D	Kielb and Kaza, 1983	46
I	Transonic	Surampudi and Adamczyk, 1986	35	2-D	(b)	
I	Supersonic (Supersonic axial)	Lane, 1957	36	2-D	Kielb and Ramsey, 1989	42
I	Supersonic (Subsonic axial)	Goldstein, Braun, and Adamczyk, 1977	33	2-D	Busbey, Kaza, and Keith, 1986	47
		Adamczyk and Goldstein, 1978	34	2-D	Adamczyk, Goldstein, and Hartman, 1978	45
					Kielb and Kaza, 1983	46
I	Subsonic	Williams, 1985	43	3-D	Kaza, et al., 1987	50
II	Potential	Verdon and Caspar, 1984	28	2-D	Smith, 1991	54
II	Euler	Hall and Clark, 1991	29	2-D	(b)	
II	Navier-Stokes	(c)		(c)	(c)	
III	Potential	Kao, 1989	26	2-D	Bakhle, Keith, and Kaza, 1989	57
		Ku and Williams, 1990	27	3-D	Ku and Williams, 1990	27
III	Euler	Huff, Swafford, and Reddy, 1991	24	2-D	Reddy, et al., 1991	62
		Srivastava, 1990	25	3-D	Srivastava, Reddy, and Mehmed, 1992	65
III	Navier-Stokes	(c)		(c)	(c)	

[a] Type I, classical linear; Type II, linear; Type III, nonlinear.
[b] To be applied.
[c] To be developed.

structural mistuning is considered. Reference 14 provides information about systems with aerodynamic mistuning.

Aeroelastic Formulation and Solution Methods

As mentioned in the Introduction, aeroelasticity involves the interaction of structures and aerodynamics. The task of an aeroelastic analysis is to combine the formulation of the structural dynamic and unsteady aerodynamic models in a consistent manner, to solve the resulting aeroelastic model for stability and forced vibration, and to interpret those results for both qualitative trends and quantitative details (fig. 4). A detailed account of the aeroelastic formulation for a multibladed structure, or a cascade, is given in reference 15, and a brief description follows.

The formulation for the multibladed structure is begun by obtaining the governing equations for N structurally uncoupled blades:

$$[M]\{\ddot{q}\} + [K]\{q\} = \{f\} \tag{1}$$

where $[M]$ is the mass matrix, $\{q\}$ is the displacement vector, $[K]$ is the stiffness matrix, and $\{f\}$ is the aerodynamic force vector; $\{f\}$ includes both motion-dependent (self-excited) aerodynamic forces which control the stability of the aeroelastic system and motion-independent aerodynamic forces (due to inlet distortion) which are responsible for the forced response. Structural damping can be included in the analysis with no additional complication. In the present formulation, structural coupling between the blades is neglected; hence, the equations for all the blades are coupled only through the motion-dependent aerodynamic forces. It should be noted further that the Coriolis effects are also neglected since most turbomachinery blades are radially aligned; studies have shown that the Coriolis effects are also negligible for propfan blades. Equations (1) can be solved in either the time or frequency domain as shown in the following sections.

Time Domain Aeroelastic Analysis

In the time domain aeroelastic analysis, the equations of motion (1) are integrated in time starting from the steady operating condition and some initial conditions. Thus the response, variation of the displacement vector $\{q\}$ with time, is obtained; a growing amplitude indicates the flutter condition. The selected steady flow condition determines whether the small initial disturbance will grow or decay. The calculation is repeated until a flow condition is found for which a constant-amplitude motion is obtained that determines the flutter boundary.

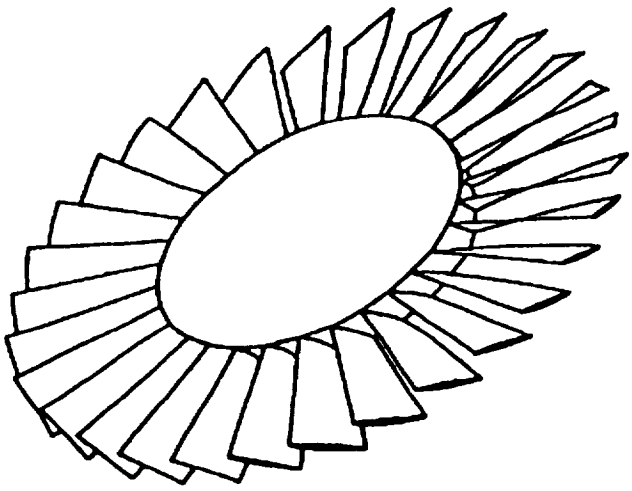

(a) Three-dimensional view.

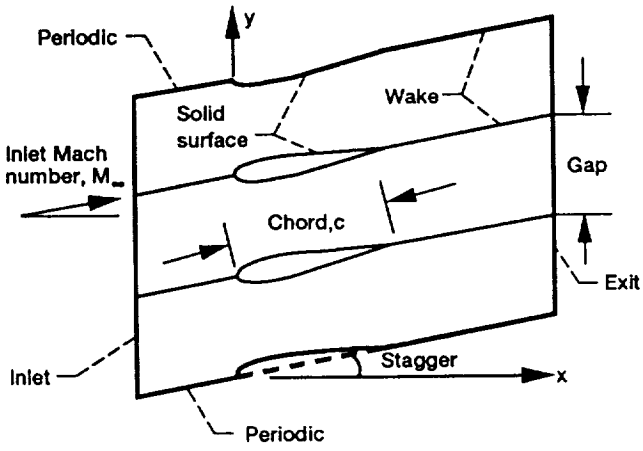

(b) Section along stream surface.

Figure 2.—A multibladed structure.

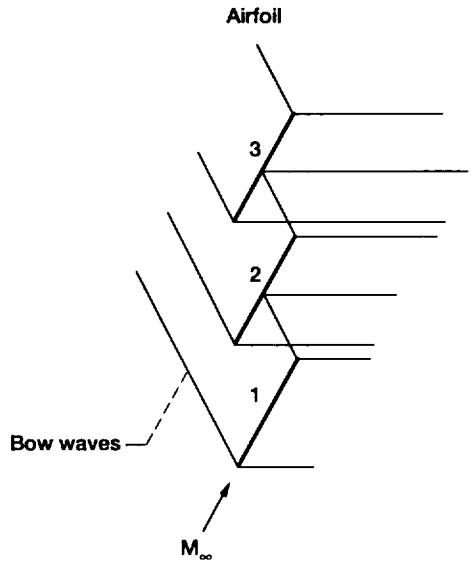

(a) Subsonic axial velocity.

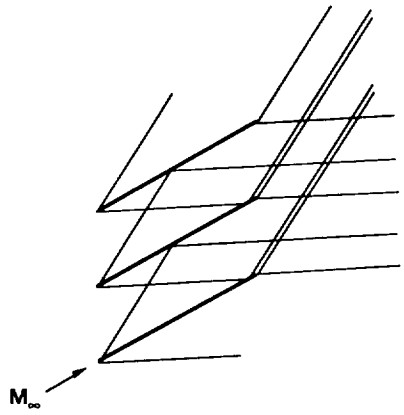

(b) Supersonic axial velocity.

Figure 3.—Cascades in supersonic relative inlet flow showing wave reflection patterns.

The various methods that can be used to integrate the aeroelastic equations in time are given in reference 16. Among these, the Newmark method introduces the least amount of numerical dissipation and error and thus gives the most accurate results. In this method, using constant acceleration between two time steps, equations (1) are discretized as follows:

$$[M]\{\ddot{q}\}_{\tau+\Delta\tau} + [K]\{q\}_{\tau+\Delta\tau} = \{f\}_{\tau} \tag{2a}$$

and

$$\{q\}_{\tau+\Delta\tau} = \{q\}_{\tau} + \Delta\tau\{\dot{q}\}_{\tau} + \left(\frac{\Delta\tau^2}{4}\right)\left(\{\ddot{q}\}_{\tau} + \{\ddot{q}\}_{\tau+\Delta\tau}\right) \tag{2b}$$

$$\{\dot{q}\}_{\tau+\Delta\tau} = \{\dot{q}\}_{\tau} + \left(\frac{\Delta\tau}{2}\right)\left(\{\ddot{q}\}_{\tau} + \{\ddot{q}\}_{\tau+\Delta\tau}\right) \tag{2c}$$

In equations (2), the subscripts τ indicate the time level at which the corresponding terms are evaluated. The structural dynamic equations are integrated using known aerodynamic forces to obtain an updated value of $\{q\}$. Then, $\{q\}$ is used as grid motion in the aerodynamic equation solver to obtain new aerodynamic forces, which in turn are used to solve for new values of $\{q\}$ and so on. The simultaneous integration of the fluid and structure equations is continued until the characteristics of the response become clear. If motion-independent aerodynamic forces are present, the time domain method automatically gives the forced response (variation of the displacement vector with time); the magnitude of the response

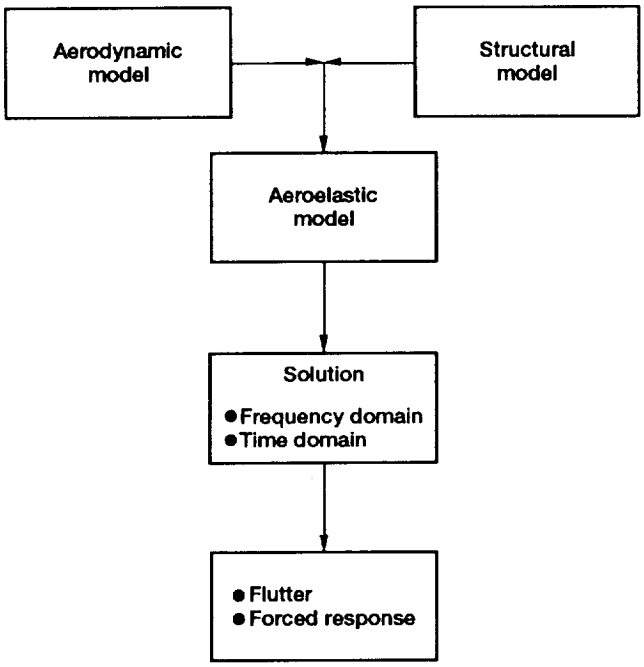

Figure 4.—Aeroelastic analysis flowchart.

can be used to calculate the stress and strain in the blades. Because the time domain method does not involve the assumption of linearity that is inherent in the frequency domain method, it allows the modeling of systems that contain structural and/or aerodynamic nonlinearities. In addition, mistuning effects due to blades with different structural properties are accounted for directly and do not need a special formulation.

Frequency Domain Aeroelastic Analysis

The frequency domain aeroelastic analysis, unlike the time domain analysis, is based on the assumption of a linear relation between forces and motion. This allows the aerodynamic force term $\{f\}$ in equations (1) to be decomposed into motion-dependent $\{f_a^q\}$ and motion-independent $\{f_a\}$ contributions as

$$\{f\} = \{f_a^q\} + \{f_a\} \tag{3a}$$

The frequency domain aeroelastic analysis assumes that it is possible to obtain aerodynamic forces for a very specific temporal and spatial motion, namely sinusoidal in time and fixed interblade phase along the cascade; that is, the n^{th} degree of freedom (n^{th} component of the displacement vector) of the s^{th} blade is written as

$$q_{ns} = \sum_r \bar{q}_{\sigma_r} e^{i(\omega t + s\sigma_r)} \tag{3b}$$

where $\bar{q}_{\sigma_r}$ is the amplitude of the traveling wave of interblade phase angle σ_r, and ω is the frequency of oscillation. In a cascade of N blades, the number of possible interblade phase angles is restricted (ref. 17) to

$$\sigma_r = 2\pi r/N \qquad r = 0,1,2,\cdots,N-1 \tag{4}$$

Then, the displacement vector for all the blades (assuming for clarity that each blade has only one displacement component) can be written as

$$\{q_s\} = [E]\{\bar{q}_{\sigma_r}\}e^{i\omega t} \tag{5}$$

where

$$[E] = \begin{bmatrix} E_{0,0} & & E_{0,N-1} \\ & \ddots & \\ E_{N-1,0} & & E_{N-1,N-1} \end{bmatrix}$$

$$E_{s,r} = e^{i2\pi sr/N}$$

Assuming that the blades are undergoing a traveling wave motion given by equation (5), the aerodynamic forces $\{f_a^q\}$ and $\{f_a\}$ can be expressed as

$$\{f_a^q\} = \pi\rho b^2\omega^2[E]\{l_{\sigma_r}\}\{\bar{q}_{\sigma_r}\}e^{i\omega t} \tag{6a}$$

$$\{f_a\} = \pi\rho b^2\omega^2[E]\{f_{\sigma_r}\}e^{i\omega t} \tag{6b}$$

where ρ is the density of the air, b is the semichord, $\{l_{\sigma_r}\}$ is the complex force coefficient due to blade motion; and $\{f_{\sigma_r}\}$ is the complex force coefficient independent of blade motion.

Equations (5) and (6) can be combined with equations (1) to yield the governing aeroelastic equations in three ways.

Traveling wave form.—The governing equations are written in terms of interblade phase angle modes by substituting $\{q\}$, $\{f_a^q\}$, and $\{f_a\}$ from equations (5) and (6) into equations (1), which results in

$$-\omega^2[E]^{-1}[M][E]\{\bar{q}_{\sigma_r}\} + [E]^{-1}[K][E]\{\bar{q}_{\sigma_r}\} = \pi\rho b^2\omega^2\{l_{\sigma_r}\}\{\bar{q}_{\sigma_r}\} + \pi\rho b^2\omega^2\{f_{\sigma_r}\} \tag{7a}$$

Individual blade form.—The governing equations are written in terms of blade displacements by expressing $\{f_a^q\}$ in $\{q_s\}$ using equation (5) and

$$-\omega^2[M]\{\bar{q}\} + [K]\{\bar{q}\} = \pi\rho b^2\omega^2[L]\{\bar{q}\} + \pi\rho b^2\omega^2\{\bar{f}\} \qquad (7b)$$

where $[L] = [E]\,[l_{\sigma_r}]\,[E]^{-1}$; $\{\bar{q}\}$ is the amplitude of the harmonic motion and $\{\bar{f}\}$ is the amplitude of the harmonic forcing function $\{f_a\}$.

Standing wave mode form.—The governing equations are expressed in sine and cosine modes or in structural eigenmodes:

$$\{\bar{q}_{\sigma_r}\} = [E]^{-1}[P]\begin{Bmatrix}\bar{q}_{cr}\\ \bar{q}_{sr}\end{Bmatrix} \qquad (8a)$$

where

$$[P] = \begin{bmatrix} C_{0,0} & C_{0,1} & S_{0,1} & C_{0,2} & S_{0,2} & \cdots \\ C_{1,0} & C_{1,1} & S_{1,1} & C_{1,2} & S_{1,2} & \cdots \\ \vdots & \vdots & \vdots & \vdots & \vdots & \vdots \\ C_{N-1,0} & \cdot & \cdot & \cdot & \cdot & S_{N-1,(N-1)/2} \end{bmatrix}$$

$$C_{s,r} = \cos(2\pi sr/N)$$

$$S_{s,r} = \sin(2\pi sr/N)$$

Substitute equations (6a), (6b), and (8a) into equations (1) to obtain the equation for the standing wave form:

$$-\omega^2[P]^{-1}[M][P]\begin{Bmatrix}\bar{q}_{cr}\\ \bar{q}_{sr}\end{Bmatrix} + [P]^{-1}[K][P]\begin{Bmatrix}\bar{q}_{cr}\\ \bar{q}_{sr}\end{Bmatrix} = \pi\rho b^2\omega^2[P]^{-1}[L][P]\begin{Bmatrix}\bar{q}_{cr}\\ \bar{q}_{sr}\end{Bmatrix} + \pi\rho b^2\omega^2\begin{Bmatrix}\bar{f}_{cr}\\ \bar{f}_{sr}\end{Bmatrix} \qquad (8b)$$

where

$$\begin{Bmatrix}\bar{f}_{cr}\\ \bar{f}_{sr}\end{Bmatrix} = [P]^{-1}\{f_a\} \qquad (8c)$$

It should be noted that in equations (7a), (7b), and (8b) the term $e^{i\omega t}$ is cancelled from both sides. Also, note that the elements of the matrix $[E]^{-1}$ are given by

$$E_{s,r}^{-1} = \frac{1}{N}e^{i\,2\pi sr/N}$$

Once the aerodynamic forces $[l_{\sigma_r}]$ and $\{f_{\sigma_r}\}$ are available for all possible values of σ_r in equation (4) (i.e., all traveling wave modes), equation (7) or (8) can be used for stability and response prediction. If $\{f_{\sigma_r}\}$ is set to zero, the equations can be cast as an eigenvalue problem and the eigenvalues can be used to determine stability. An energy approach can also be used to infer aeroelastic stability. If $[l_{\sigma_r}]$ is set to zero, equation (7) or (8) results in an algebraic expression from which the response can be calculated by simple matrix inversion and multiplication. The responses can be summed up to get the total response, and they can be used in calculating stress or strain on the blades.

Structural Models

The various structural models developed thus far are shown in figure 5. However, the nature of the formulation given in the previous sections allows any other model to be included in the aeroelastic analysis provided that the mass and stiffness matrices are known.

Typical Section Model

The structural model for a cascade consists of a typical section with two degrees of freedom (bending and torsion) for each blade (see fig. 5(a)). The equations of motion for the s^{th} blade are

$$m\ddot{h} + S_\alpha\ddot{\alpha} + K_h h = f_h \qquad (9a)$$

$$S_\alpha\ddot{h} + I_\alpha\ddot{\alpha} + K_\alpha\alpha = f_\alpha \qquad (9b)$$

where m is the airfoil mass, h is the plunging (bending) displacement, S_α is the static unbalance, α is the pitching (torsion) displacement, I_α is the moment of inertia, K_h and K_α are the spring constants for plunging and pitching, respectively, f_h and f_α are the aerodynamic loads (including both motion-dependent and motion-independent contributions), and the dots over the various terms indicate differentiation with respect to time. A structural damping term can be included in the analysis with very little additional complication.

The aeroelastic formulation in the frequency domain, based on a traveling wave form (eqs. (6)), is detailed in reference 18 for both tuned and mistuned cascades; the procedures for determining stability and forced response are also discussed. These are repeated in the appendix for completeness. Even though the formulation is presented for a typical-section structural model with two degrees of freedom, the same formulations can be used with other structural models described in the following sections.

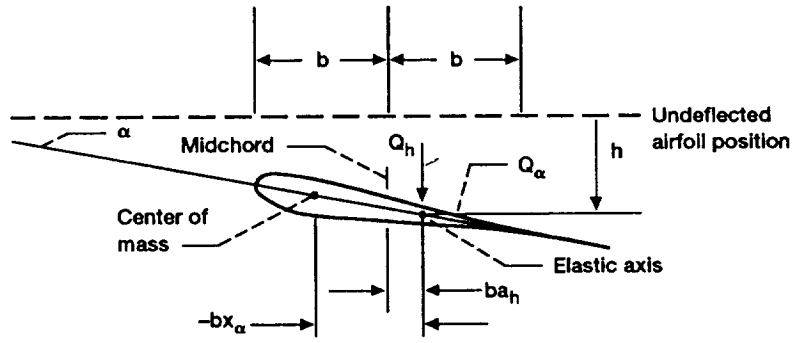

(a) Typical-section model.

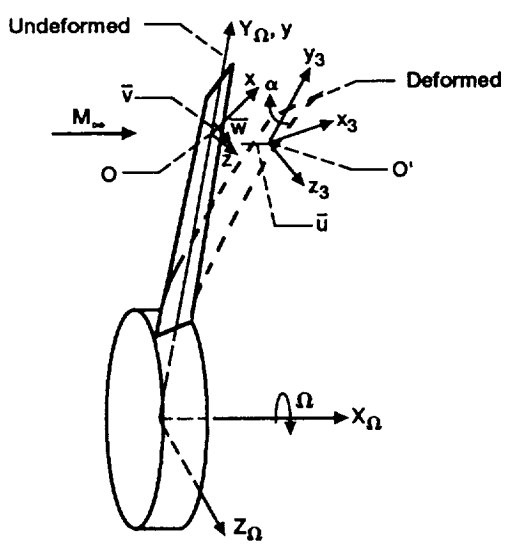

(b) Beam model with rigid disk.

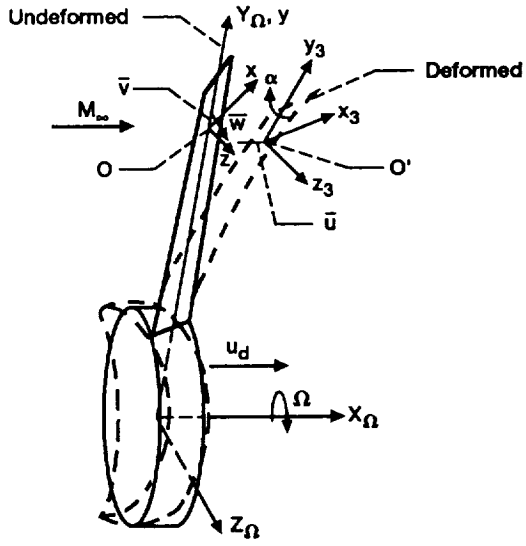

(c) Beam model with flexible disk.

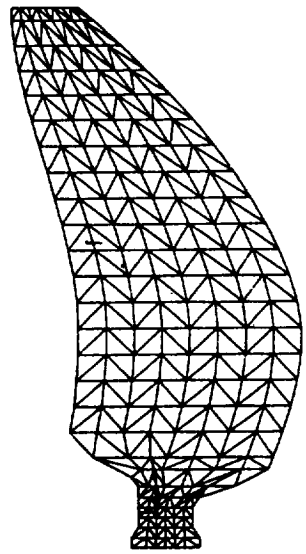

(d) Finite-element model.

Figure 5.—Structural models.

Beam Model (Ref. 19)

The beam structural model of each blade consists of a straight, slender, twisted, elastic beam with a symmetric varying cross section (fig. 5(b)). The elastic, the inertia, and the tension axes are each taken to be noncoincident. The effect of warping is not explicitly considered. The blade is assumed to be rigid in the radial direction. Consequently, the radial component of the equations of motion is eliminated. The structural model has its basis in the geometric nonlinear theory of elasticity in which elongations and shears are negligible compared with unity, and the squares of the derivatives of the deformation of the elastic axis are negligible compared with the squares of the bending slopes. This level of the geometric nonlinear theory of elasticity is required to derive a set of linear coupled bending-torsion equations of motion.

The blade degrees of freedom consist of bending in the plane of rotation $\bar{u}$, bending in the plane perpendicular to the plane of rotation $\bar{w}$, and pitching (torsion) about the elastic axis, α, as shown in figure 5(b). In deriving the equations of motion, three coordinate systems are used (fig. 5(b)). The $X_\Omega, Y_\Omega, Z_\Omega$ is the hub fixed system and rotates about the Z_Ω axis with an angular velocity Ω; x, y, z is the blade fixed system at an arbitrary point 0 on the elastic axis, and x_3, y_3, z_3 is the blade fixed system at 0′ after deformation, obtained by rotating xyz by α. The equations of motion are derived using the extended Hamilton's principle. By substituting expressions for strain energy, kinetic energy, and virtual work of aerodynamic forces and by performing the required operations, the governing equations are obtained. The primary motions are expanded in terms of the generalized coordinates $\{q\}$, associated with the nonrotating uncoupled beam modes in pure bending and torsion, to obtain the governing equations in the form shown in equations (1). The elements of $[M]$ and $[K]$ are defined in reference 18. Thus, formulations for both tuned and mistuned systems can be written in a form similar to those presented for the typical-section model.

Bladed-Disk Model (Ref. 20)

The bladed-disk system is idealized as a constant-thickness, uniform circular disk to which the blades are attached; only the disk out-of-plane bending motion u_d is considered (fig. 5(c)). With the exception that the warping of the blade cross sections is explicitly considered, the blade model is the same as that discussed in reference 19 and explained in the section Beam Model. The equations are written in traveling wave form for the blades (eqs. (7)) and in standing wave form for the disk (eqs. (8)). Continuity and slope continuity are enforced at the blade-disk junction. Hamilton's principle is again used to obtain the matrices $[M]$ and $[K]$.

Finite-Element Model (Ref. 21)

Although the models just described help in understanding the basic aeroelastic problem, a finite-element model (fig. 5(d)), is often required to accurately represent more complex blade structures such as propfan blades. Because propfan blades are thin and flexible, deflections due to centrifugal and aerodynamic loads are large. Hence, the aeroelastic problem is inherently nonlinear, requiring the geometric nonlinear theory of elasticity. The blades of a propfan have a low aspect ratio and they behave as platelike structures having chord flexibility and requiring a three-dimensional structural model. They have large sweep and twist, which couples blade bending and torsional motions. These factors require a finite-element structural model that also accounts for centrifugal softening and stiffening effects. Using finite-element models, the governing equations can be written again as shown in equations (1). The matrices $[M]$ and $[K]$ are obtained from the finite-element analysis. Again, these can be used in the aeroelastic formulation with appropriate aerodynamic models. For most of the studies at Lewis, a NASTRAN finite-element analysis is used. A review of the available finite elements in COSMIC/NASTRAN and MSC/NASTRAN, along with their capabilities and limitations for modeling flexible rotating blades, is given in reference 22; reference 23 describes the geometric nonlinear analysis using MSC/NASTRAN for frequency and mode shape calculation of blades under centrifugal loading.

Aerodynamic Models

The various aerodynamic models used at Lewis are presented in table I. Nonlinear models (refs. 24 to 27), referred to as Type III models, include the effects of the blade shape and thickness. In addition, the nonlinear models are not restricted to small-amplitude blade oscillations so the assumption of sinusoidal motion is not required. These models are valid for arbitrary motion but require more computing time. Two types of linear unsteady cascade analyses have been developed on the assumption that the unsteady disturbance is small. One analysis (Type II) linearizes about a nonuniform, deflected mean flow (refs. 28 and 29); the other (Type I) linearizes about a uniform, undeflected mean flow (refs. 30 to 36). In the present report, Type II models are referred to as linear models and Type I models as classical linear models. Since these linear models are based on a small perturbation analysis, nonlinearities related to the amplitude of motion are not modeled in either analysis.

Type III (Nonlinear) Models

The nonlinear models require the numerical solution of the equations of fluid dynamics. In reality, both steady and unsteady flows in turbomachines and propfans are extremely complicated. The fluid is viscous and heat conducting and is most accurately described by the Navier-Stokes equations. However, if the Reynolds number is sufficiently high and separation does not occur, then the viscous and heat-transfer effects are confined to narrow regions near the airfoil surfaces and the wakes. Under these circumstances, the Euler equations provide a good approximation of the behavior of the flow. The three-dimensional Euler equations in a Cartesian frame are given as

$$\frac{\partial Q}{\partial t} + \frac{\partial E}{\partial x} + \frac{\partial F}{\partial y} + \frac{\partial G}{\partial z} = 0 \tag{10}$$

where

$$Q = [\rho, \rho u, \rho uv, \rho w, e]^{\mathrm{T}} \tag{11a}$$

$$E = \left[\rho u, \rho u^2 + p, \rho uv, \rho uw, u(e+p)\right]^{\mathrm{T}} \tag{11b}$$

$$F = \left[\rho v, \rho uv, \rho v^2 + p, \rho vw, v(e+p)\right]^{\mathrm{T}} \tag{11c}$$

$$G = \left[\rho w, \rho uw, \rho vw, \rho w^2 + p, w(e+p)\right]^{\mathrm{T}} \tag{11d}$$

and ρ is the fluid density, u, v, and w are the Cartesian velocity components, e is the energy per unit volume, and p is the fluid pressure. Appropriate boundary conditions can be specified to complete this formulation.

Generally, equations (10) in conservative differential form are transformed from a Cartesian reference frame to a time-dependent, body-fitted curvilinear reference frame for numerical solution. The transformed two-dimensional Euler equations are solved using the flux-difference-splitting (FDS) scheme in reference 24. The three-dimensional Euler equations are solved using the alternating-direction-implicit (ADI) scheme for propfan configurations in reference 25.

For irrotational flow, the full potential equation is obtained from the Euler equations:

$$\frac{\partial \rho}{\partial t} + \frac{\partial(\rho u)}{\partial x} + \frac{\partial(\rho v)}{\partial y} + \frac{\partial(\rho w)}{\partial z} = 0 \tag{12}$$

where

$$u = \frac{\partial \phi}{\partial x} \qquad v = \frac{\partial \phi}{\partial y} \qquad w = \frac{\partial \phi}{\partial z}$$

$$\frac{\rho}{\rho_\infty} = \left(1 + \frac{(\gamma-1)}{2}\left\{M_\infty^2 - \left[2\frac{\partial \phi}{\partial t} + \left(u^2 + v^2 + w^2\right)\right] / a_\infty^2\right\}\right)^{1/(\gamma-1)}$$

In the preceding equations, ϕ is the velocity potential; ρ_∞, a_∞, and M_∞ are the density, sonic velocity, and Mach number, respectively, at the reference condition. Kao (ref. 26) solved the two-dimensional version of the full potential equation in finite-volume form by using the Newton iteration method for a cascade of blades. The three-dimensional equations for propfan configurations have been solved by Ku and Williams (ref. 27).

The nonlinear unsteady aerodynamic models allow either a frequency domain or a time domain aeroelastic analysis to be performed using the same aeroelastic solver. Since the frequency domain flutter analysis is linear in nature, the use of a nonlinear unsteady aerodynamic model in a frequency domain flutter calculation may seem inconsistent, but it is justified in the absence of a corresponding linear aerodynamic solver. The unsteady harmonic force coefficients required in the frequency domain analysis can be obtained by harmonically oscillating the blades and by Fourier-decomposing the resulting forces. However, this process is time consuming in comparison with those of the Type I and Type II models in which a harmonic variation of the flow variables is assumed, thus removing the time dependency. In order to make the time-accurate nonlinear codes more computationally efficient, two methods have been developed and implemented in the codes: the Influence Coefficient and Pulse Response methods (ref. 37). These methods are valid for small-amplitude blade oscillations for which the unsteady flow field is linearly dependent on the amplitude. Other methods of reducing computational time such as parallel processing (ref. 38) and reduced-order modeling for flutter analysis (ref. 39) are also pursued at Lewis. These methods reduce the computational time required and allow the nonlinear codes to be used efficiently for a linear frequency domain analysis while the flexibility of a time domain analysis is maintained.

In addition, viscous terms can be easily included in the nonlinear Euler equations and can be used for accurate prediction of stall and choke flutter (see fig. 1(a)), which involve nonlinear behavior. Earlier methods have used empirical models to investigate these types of flutter (refs. 40 and 41).

Type II (Linear) Models

Type II models use full nonlinear equations for the steady solution but use linearized equations for the unsteady solution (refs. 28 and 29). Thus, the effect of airfoil shape and angle of attack can be included in the unsteady aerodynamic and aeroelastic calculations.

The model developed by Verdon and Caspar (ref. 28) is based on the two-dimensional potential equation. The potential function is expanded in a perturbation series as

$$\phi(x,y,t) = \phi_0(x,y) + \varepsilon\phi_1(x,y,t) + \ldots \qquad (13)$$

where ε is a small parameter. Substituting back into the governing equation (eq. (12)) and neglecting terms of $0(\varepsilon^2)$, a nonlinear equation in ϕ_0 for steady flow and a linear variable-coefficient equation in ϕ_1 for unsteady flow are obtained. The equation for steady flow is the steady nonlinear (full) potential equation; this equation is solved in order to obtain the steady flow field, which in turn is used to calculate the coefficients in the unsteady equation. A further simplification is made by assuming that the flow field varies harmonically with time. This assumption allows a single interblade passage of the cascade to be used for calculations with any interblade phase angle and also removes the time dependence from the formulation. Hall and Clark (ref. 29) developed a similar model based on two-dimensional Euler equations. Three-dimensional models are in a developmental stage.

Type I (Classical Linear) Models

In Type I models, the unsteady potential flow is linearized about a uniform mean flow; that is, ϕ_0 is linear. Thus, the effects of blade shape (airfoil thickness and camber) are neglected entirely (refs. 30 to 36). These models can be applied only to cases in which the effects of blade geometry can be neglected. Whitehead, Smith, and Rao and Jones (refs. 30 to 32) solved the two-dimensional linear potential equation for subsonic flow by using different numerical techniques. Goldstein, Braun, and Adamczyk (refs. 33 and 34) solved the linear potential equation for supersonic flow with a subsonic leading edge locus. Surampudi and Adamczyk (ref. 35) solved the equations for nominally sonic flows. The formulation by Lane (ref. 36) is coded into a program by Kielb and Ramsey (ref. 42) for solving supersonic flow with a supersonic axial component. A formulation based on linear compressible small-disturbance theory was developed for a three-dimensional rotating multibladed geometry (ref. 43). In this work, an integral equation relating the normal velocity to the load distribution on the blade is derived. The integral equation is solved by dividing the blade into a finite number of elements (panels) on each of which the load is constant. The loads on all the elements are determined simultaneously by requiring that the normal induced velocity be equal to the specified value at the control point. This formulation was recently extended to single-rotation propfans with ducts (ref. 44).

Results and Discussion

The structural and aerodynamic models described in the previous sections were applied to investigate the aeroelastic stability and response of wind tunnel propfan models. The following selected results are a comparison of analyses and experimental measurements. It should be noted that the analyses are limited to isolated blade rows or to single-rotation (SR) propfans. Table II presents the propfan configurations that were referenced in this report.

Type I (Classical Linear) Aerodynamic Models

The earliest aeroelastic model was the typical-section structural dynamic model with plunging and pitching motions of each blade along with a two-dimensional linear cascade aerodynamic model. This model was used as a research tool to understand the physics of cascade effects.

TABLE II.—PROPFAN CONFIGURATIONS

Model	Configuration	Tip geometric sweep, deg	Number of blades in full rotor, N	Material	Reference diameter m (in.)	Ratio of hub to blade diameter
SR3	Single rotation	45	8	Titanium	0.622 (24.5)	0.239
SR3CX2	↓	45	8	Composite	.622 (24.5)	.239
SR3C-3		45	8	Composite	.622 (24.5)	.239
SR5		60	10	Titanium	.622 (24.5)	.235
SR7L		41	8	Composite shell/ titanium spar	2.74 (108)	.232
SR7A	↓	41	8	↓		
F21	Counter rotation (forward rotor)	45	13	↓	.622 (24.5) .617 (24.3)	.232 .430

Researchers who investigated flutter in tuned rotors in supersonic flow with a subsonic leading edge locus used an energy approach to infer the stability (ref. 45). The flutter analysis was applied to compressors at both high and low backpressure conditions by using the theories of references 33 and 34, respectively. The calculated stability trends were consistent with experimental rig observations. In reference 18, the typical-section model was also used to understand the effects of mistuning; an eigenvalue approach was employed to determine stability. The results obtained using this aeroelastic model showed that bending-torsion coupling has a significant effect on cascade flutter. Also noted was that frequency mistuning had a beneficial effect on suppressing flutter in all the flow regimes considered (refs. 18, 42, 46, and 47) and that it had either a beneficial or an adverse effect on forced response. These results were later used as benchmarks for checking more complicated models.

Subsequently, the beam structural model was used along with a two-dimensional aerodynamic model applied in a stripwise fashion (ref. 19). Disk flexibility was included in the aeroelastic formulation in reference 20. Parametric studies indicated that the effect of frequency mistuning on flutter was still beneficial even in the presence of structural coupling between blades due to disk flexibility. Also, it was found that blade pretwist introduces strong coupling between the disk bending and blade chordwise motions.

The beam model was used to predict and correlate the flutter speed of the SR5 propfan wind tunnel model and to clarify the mechanism of the flutter phenomenon (ref. 5). This beam model was modified to account for blade sweep in an approximate manner as shown in figure 6. The two-dimensional aerodynamic models were also modified to account for sweep by using similarity laws. The disk was assumed to be rigid. Figure 7 shows the calculated flutter boundary in comparison with experimental data. The measured and calculated flutter boundary trends are seen to be in good agreement, as were the flutter frequencies. Also, the flutter interblade phase angles agreed well with the calculations. However, because the analytical results required judgement in selecting an effective blade sweep and a blade elastic axis position, a three-dimensional finite-element structural model was developed to circumvent making such a decision.

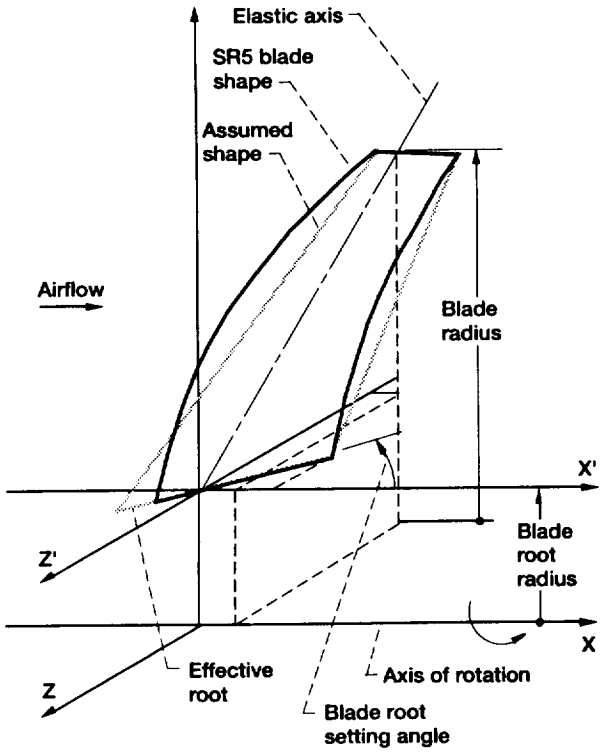

Figure 6.—Swept beam model (ref. 5).

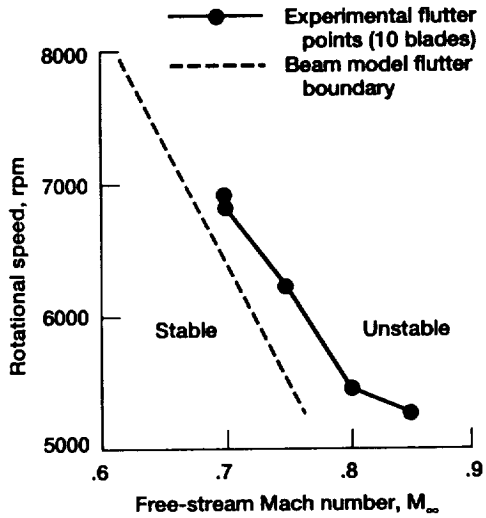

Figure 7.—Comparison of beam model flutter boundary and experimental flutter points for SR5 propfan (ref. 5).

A finite-element structural model and a three-dimensional aerodynamic model were applied to correlate the flutter boundary of the SR3CX2 propfan (ref. 21). A NASTRAN finite-element model was used to obtain the mode shapes and frequencies of the propfan. The three-dimensional linear aerodynamic model of reference 43 was used. The calculated shapes and frequencies of the first two natural modes are shown in figure 8(a). The mode shapes include the effect of centrifugal load. The following findings were made: the first mode was primarily bending and the second mode primarily torsion; centrifugal loads increased blade twist and aerodynamic loads decreased twist; the combined loads resulted in a net increase in twist, and this twist increased with rotational speed. In comparison with measured flutter data, the calculated flutter results are presented in figure 8(b) for four and eight blades. The difference between the calculated and measured flutter Mach numbers was greater for the four-blade case than for the eight-blade case, which implies that the theory may not be accurate for large blade spacing. Calculated and measured interblade phase angles also compared well; however, the calculated flutter frequencies

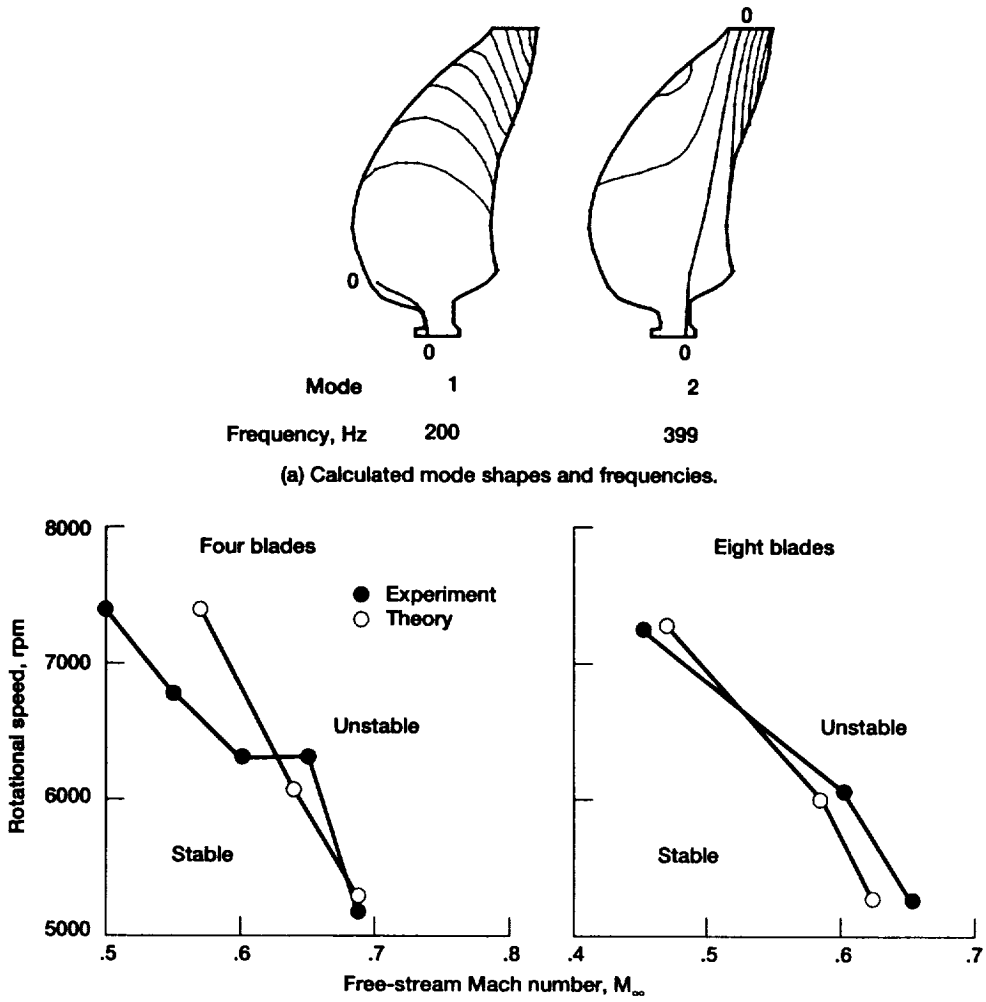

(a) Calculated mode shapes and frequencies.

(b) Measured and calculated flutter boundaries.

Figure 8.—SR3CX2 propfan mode shapes, frequencies, and flutter boundaries at blade setting angle $\beta = 61.6°$ (ref. 21).

were about 8 percent higher than the measured. Calculations were also performed using the three-dimensional structural model with two-dimensional aerodynamic models applied in a stripwise (quasi-three-dimensional) manner for the eight-blade configuration. The correlation varied from poor to good as shown in figure 9. Recently, this quasi-three-dimensional aeroelastic analysis program was used to design flutter-free cruise missile propfans for a joint Navy/Air Force/NASA project (ref. 48). A similar quasi-three-dimensional aeroelastic analysis was also implemented in a NASTRAN analysis (ref. 49).

A three-dimensional aeroelastic model was used to perform the calculations for a propfan having alternate blade mistuning (alternate blades have different structural properties). These calculations are presented in reference 50. The propfan had four SR3CX2 blades and four SR3C–3 blades which differ in natural frequencies and mode shapes. The measured and calculated flutter boundaries are shown in figure 10. The overall agreement between theory and experiment is good.

The three-dimensional unsteady aerodynamic model (ref. 43) has the capability of performing a modal forced-response vibration analysis including structural and aerodynamic mistuning; the excitation is aerodynamic in origin. August and Kaza (ref. 51) analyzed an aeroelastically scaled model, SR7A, which was used to simulate a large-scale propfan, SR7L; the performance, vibration, forced response and flutter of both propfans were studied. They concluded that the aeroelastic model accurately simulated the prototype fan. The measured and calculated one-per-revolution, forced vibratory stress amplitudes for the root region of the SR5 propfan blade are shown in figure 11 (from ref. 52); the calculations are based on the three-dimensional unsteady aerodynamic model. Good correlation between experiment and analysis is seen; the correlation for the tip region (not shown here) is not as good. The flutter predictions for SR5 from reference 13 are shown in figure 12. The maximum difference between theory and experiment was 16.7 percent at 6800 rpm, and the numerical predictions are seen to be unconservative. It should be noted that, even

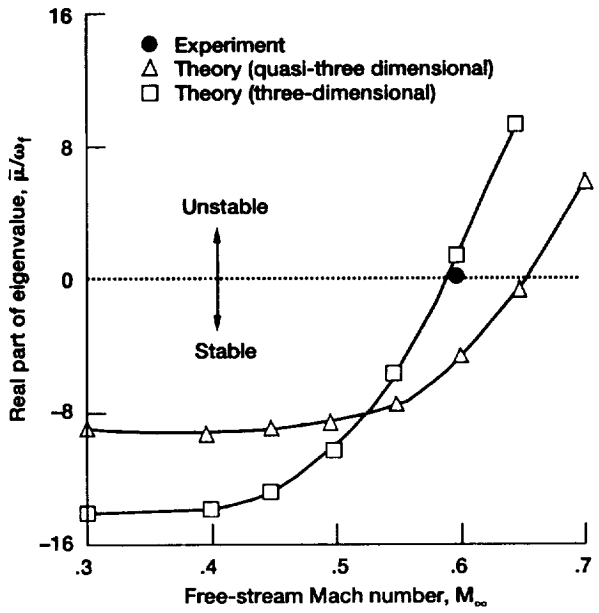

Figure 9.—Flutter results from quasi-three dimensional and three-dimensional aeroelastic models for SR3CX2 propfan (ref. 21).

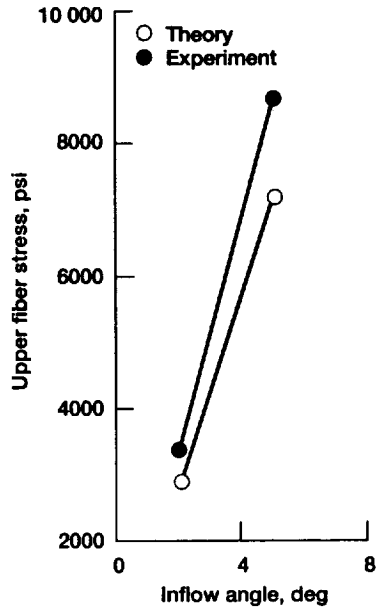

Figure 11.—Vibratory stress amplitudes for SR5 propfan based on three-dimensional aerodynamic model (ref. 52); Mach number, 0.8; rotational speed, 5500 rpm.

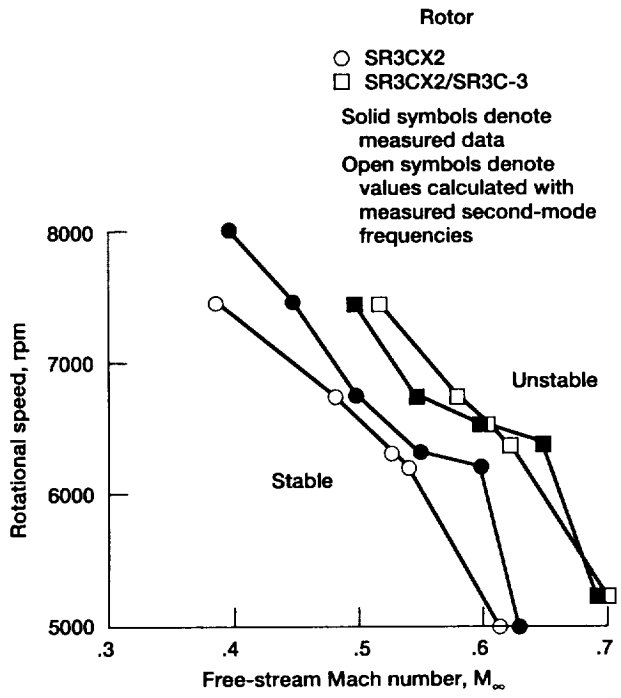

Figure 10.—Flutter boundaries for mistuned propfan (ref. 50).

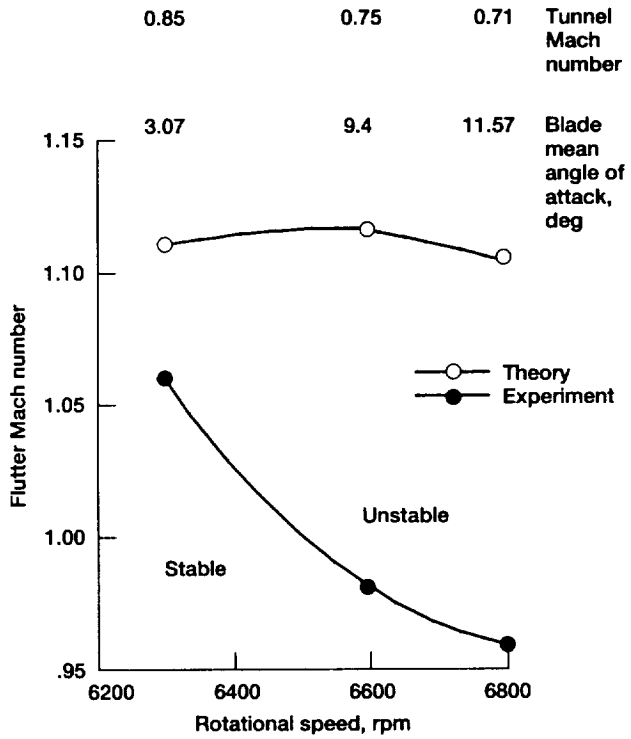

Figure 12.—Flutter boundaries for SR5 propfan (ref. 13) at blade setting angle $\beta_{0.75R} = 69.3°$.

though both stress and flutter predictions fall within 20 percent of the experimental data, the stress prediction will result in a safe design whereas the flutter prediction will result in an unsafe design. The observed differences indicate the need for more accurate modeling in the tip region and for the modeling of transonic flow, which would require advanced aerodynamic models (Types II and III).

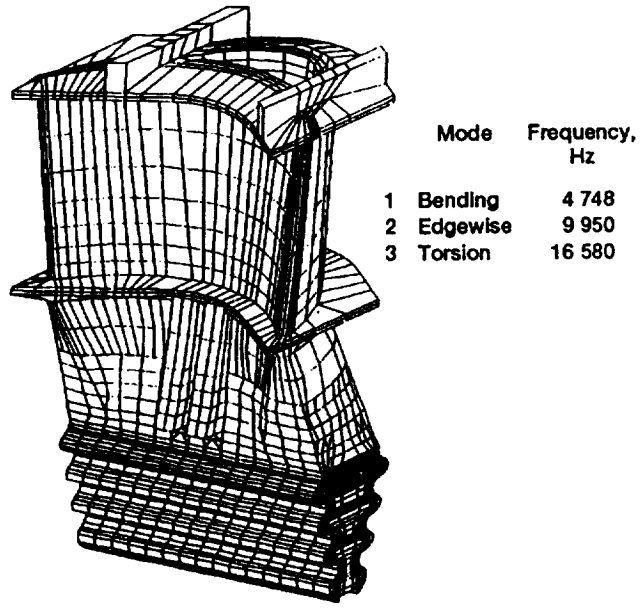

(a) Finite-element model and natural frequencies; 10014 nodes; 7758 brick elements.

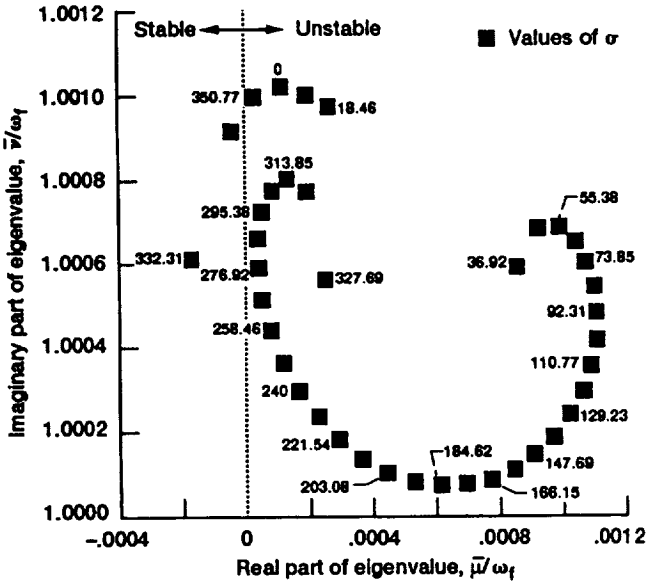

(b) Root locus plot from two-dimensional linearized potential solver for vibration in second (edgewise) mode, zero structural damping.

Figure 13.—Space shuttle main engine (SSME) high-pressure-oxygen turbopump (HPOTP) turbine aeroelastic analysis (ref. 54).

Type II (Linear) Aerodynamic Models

As can be seen from table I, the only aeroelastic application of the Type II aerodynamic model is the one based on the two-dimensional linearized potential solver (ref. 28). This model improves upon the classical linear aerodynamic models used in the previous section in the following two ways. The effects of airfoil shape and angle of attack are included in the aerodynamic model, which has the capability of treating arbitrary modes including those with chordwise flexibility. A typical-section structural model was used to study the effect of steady aerodynamic loading on the flutter of a compressor cascade (ref. 53). The study showed that the neglect of steady aerodynamic loading in flutter calculations could result in nonconservative estimates of the flutter boundary. This aerodynamic model was also applied to investigate the stability and forced response of the space shuttle main engine (SSME) high-pressure-oxygen turbopump (HPOTP) turbine (ref. 54). The blades in the first stage of the turbine experienced frequent cracking in the shank region. The aeroelastic analysis was formulated in modal form, and the aerodynamic model was applied in stripwise fashion. The MSC/NASTRAN finite-element program was used to perform the structural dynamic analysis of the HPOTP turbine blade. The model consisted of 10 014 nodes and 7758 solid brick elements, as shown in figure 13(a) along with calculated natural frequencies. The span of the blade was divided into eight strips at each of which a two-dimensional linearized aerodynamic analysis was then applied. The flutter analysis indicated that the HPOTP turbine blades experienced very low aerodynamic damping in the first four vibrational modes. The second mode (first edgewise mode) was unstable (fig. 13(b)). An addition of 1 percent damping made the system stable. A mistuning analysis of the HPOTP blade (ref. 55) showed that, when small mistuning (of the order present in actual rotors) was introduced, the aeroelastic modes become localized to a few blades, possibly leading to blade failure. Some preliminary calculations of the HPOTP blade forced response due to gust and cooling jet were presented in reference 56.

Type III (Nonlinear) Aerodynamic Models

The nonlinear models were developed to investigate complicated flows involving shocks and nonlinearities in the flow. However, these models were validated in various limiting cases by comparison with linear and classical linear theory. The two-dimensional full potential equation was used to predict and validate flutter calculations for selected cases in references 57 to 60. In reference 58, a typical-section structural model was used to simulate the SR5 propfan. The aeroelastic equations were solved both in time and frequency domains. In the calculations, the cascade had five blades and the Mach number at the inlet was 0.7. Figure 14(a) shows the root locus plot with all 10 eigenvalues, 2 for each of the 5 blades in the cascade, at a reduced frequency $k_c = 0.225$. The eigenvalues fall into two groups. In the group at the lower frequency, the most unstable phase angle is 288°.

A time domain solution was also obtained by the integration of the equations of motion for each blade. Figure 14(b) shows the variation of the center blade pitching displacement

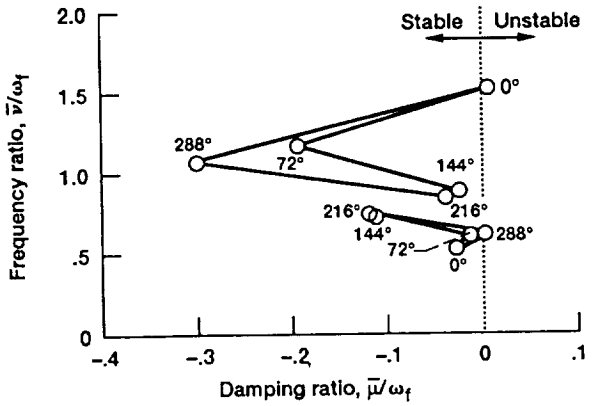

(a) Frequency domain solution for $k_c = 0.225$ ($k_c = \omega_c/M_\infty a_\infty$).

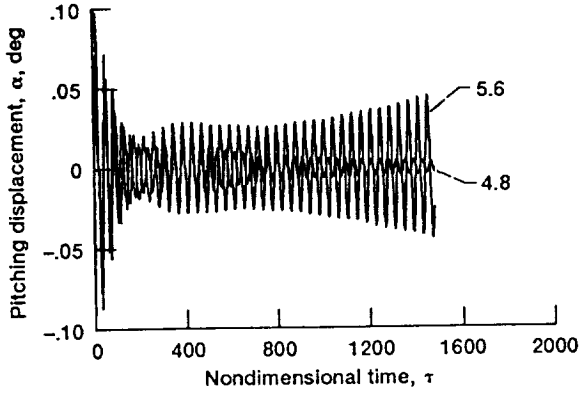

(b) Time domain solution for two values of reduced velocity $V^* = M_\infty a_\infty/b\omega_\alpha$.

Figure 14.—Flutter calculations for simulated SR5 propfan typical-section model from two-dimensional full potential solver; Mach number, 0.7 (ref. 58).

with time for stable and unstable conditions. The flutter velocity, frequency, and interblade phase angle showed good agreement with the corresponding results from the frequency domain method, thus verifying both the time and frequency domain aeroelastic analysis methods. The variation of the flutter velocity with mach number to predict the transonic dip is presented in reference 59. It was found that the transonic dip in cascades is similar to that for isolated airfoils (ref. 61), except that it occurs at significantly lower Mach numbers (see fig. 15). In reference 27, the three-dimensional full potential solver was used to analyze SR3CX2 propfan, for in-phase motions ($\sigma = 0°$) both in the time and frequency domains. The calculations and the experiments showed the blades to be stable.

The two-dimensional Euler solver was applied to calculate the flutter behavior of selected typical-section models in references 62 and 63. A calculation of the flutter condition for the SR5 propfan model produced the same results as those calculated by the full potential solver; these results are

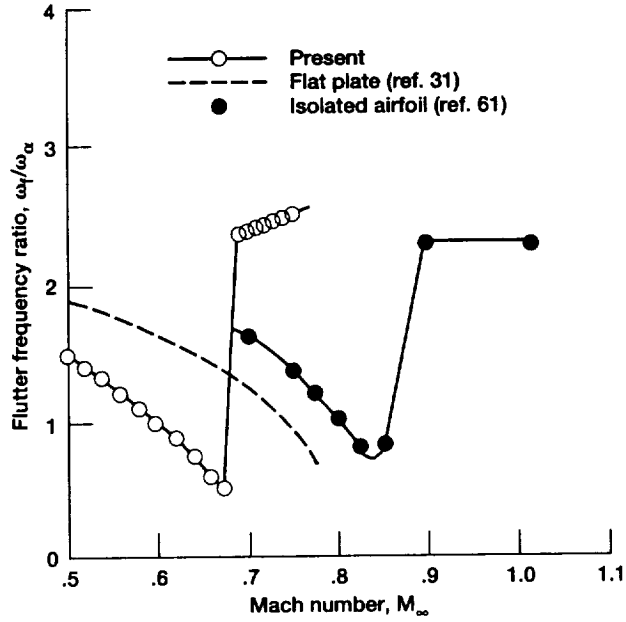

Figure 15.—Transonic dip for cascade with NACA 64A010 airfoil using full potential aeroelastic solver (denoted as "present") with comparisons to classical linear theory and isolated airfoil theory (ref. 59).

summarized in table III. The ability to predict transonic flow is demonstrated in figure 16 for an example NACA 0006 cascade (ref. 28). This figure shows the steady pressure distribution and a comparison with a full potential equation solution. The Euler equations predict the shock location slightly downstream from that predicted by the full potential solver. The unsteady pressure distribution is compared with a classical linear analysis in figure 17. This comparison shows the effect of airfoil shape on the unsteady loading and clearly indicates that classical linear theories which neglect the effects of airfoil shape are inadequate for transonic flow calculations.

The three-dimensional Euler equations were used in reference 64 to study the effect of structural flexibility on the performance of SR7L propfan, by coupling the Euler aerodynamic solver with a NASTRAN finite-element analysis. It was concluded that the customary way of adjusting the blade setting angle by rigid-body rotation does not correctly simulate the actual blade shape during operation. The

TABLE III.—COMPARISON OF FLUTTER BOUNDARIES CALCULATED FROM FULL POTENTIAL AND EULER SOLVERS[a]

Parameter	Full potential	Euler
Interblade phase angle, σ, deg	288	288
Reduced frequency, $k_c = \omega c/M_\infty \alpha_\infty$	0.225	0.222
Frequency ratio, ω/ω_α	.61	.67
Reduced velocity, $V_f = M_\infty \alpha_\infty / b\omega_\alpha$	5.43	6.10

[a] References 58 and 63.

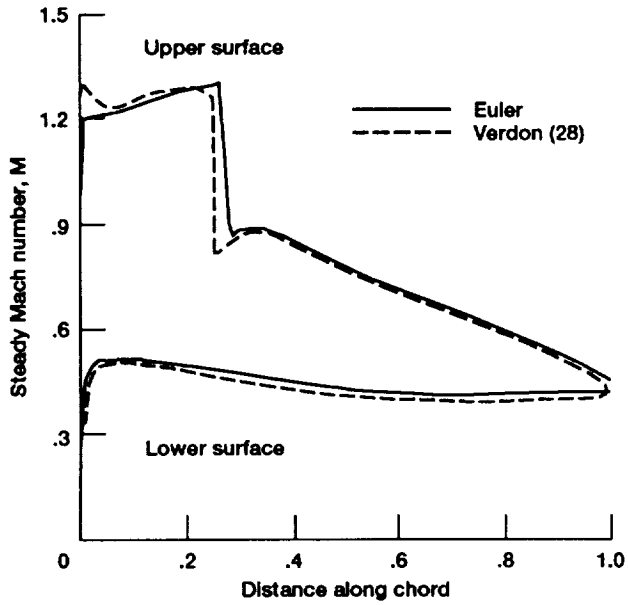

Figure 16.—Steady Mach number distribution for transonic cascade; gap-to-chord ratio, 1.0; stagger angle, 45°; relative Mach number, 0.8; incidence angle, 13° (ref. 63); full potential solution is denoted as Verdon (28) in the key.

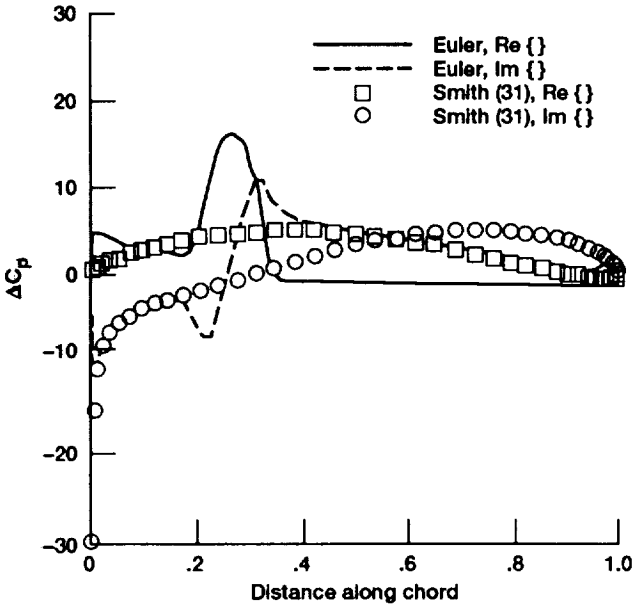

Figure 17.—Unsteady pressure distribution for transonic cascade; pitching about midchord; parameters as in figure 16 (a); reduced frequency (based on semichord) of 0.5, interblade phase angle of 0°, amplitude of oscillation of 2° (ref. 63); linear theory results are denoted as Smith (31) in the key.

three-dimensional Euler equations were also solved in reference 65 to verify the static stability characteristics of two forward-swept propfan blades. The analysis confirmed the static stability behavior of the blades that were designed with uncoupled aerostructural analysis. The study also confirmed that a forward-swept blade can be designed to be statically stable by tailoring the structural properties of the blades using composites.

Flutter calculations have been performed for the F21 propfan using both the three-dimensional full potential and Euler solvers. Neither of the codes predicted the observed flutter of the F21 propfan in the in-phase (zero interblade phase angle) mode. The presence of a leading edge vortex at the experimentally observed flutter condition is considered significant in this case. The full potential formulation does not allow the modeling of such a vortex. Preliminary Euler calculations show the presence of a leading edge vortex. Further verification using finer grid spacings is required before accurate flutter predictions can be made including the influence of the vortex. Both the full potential and Euler aeroelastic solvers, which were previously restricted to in-phase blade motions, have been extended to allow the modeling of multiple blade passages with independent blade motions. This will allow further validation of these solvers using experimental data not limited to the in-phase flutter mode.

APPLE

The structural and aerodynamic models and the time and frequency domain solution methods that have been developed and validated are being incorporated in a user-oriented program with a common data base for input and output. The acronym for this program is APPLE (Aeroelasticity Program for Propulsion at LEwis). A flowchart of this system is shown in figure 18. A graphical user interface will provide the researcher or analyst with an easy way of selecting the desired aeroelastic model suitable

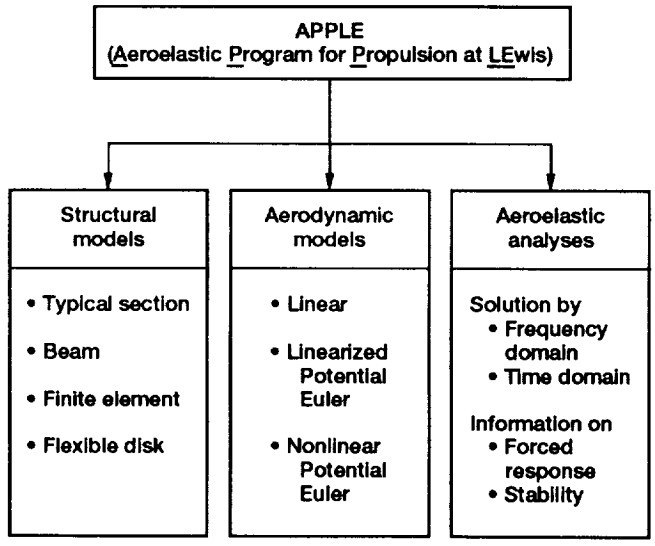

Figure 18.—Various options available in APPLE system.

for his/her purpose. This program, when completed, will run on a number of distributed workstations using parallel processing, a graphical user interface, and concurrent engineering methods. The APPLE system, when developed, can be directly integrated in the Numerical Propulsion Systems Simulator (NPSS) project being developed at NASA Lewis.

Summary of Results

A review of the aeroelastic models available for propulsion components at the NASA Lewis Research Center was presented. It is evident from this material that a number of aeroelastic models and methods exist for investigating flutter and the forced response of isolated blade rows and single-rotation propfans. The models developed thus far were valid, though restricted to single-rotation propfans, for a variety of operating conditions.

Recommendations

The following suggestions are made for future research:

(1) A comprehensive study is required to verify and evaluate the transonic modeling capability of nonlinear aeroelastic analyses for transonic flutter prediction.

(2) The development and aeroelastic application of three-dimensional linearized (Type II) aerodynamic models, based on both the potential and Euler equations, is required.

(3) All the models surveyed in this paper were restricted to inviscid flows in which viscous effects were neglected. For applications in which viscous effects are expected to be significant, viscous flow models need to be developed.

(4) Methods to predict aerodynamic forces due to inlet distortions, incident pressure waves, and other forcing functions need to be developed.

(5) Stall flutter and choke flutter remain significant problems in the design and operation of axial compressors and fans. In the past, empirical models have been used to analyze these types of flutter. Type III viscous and transonic flow models need to be developed to predict these types of flutter without using empiricism.

(6) Results presented in this report revealed that flutter usually occurred in the first two or three modes (i.e., low-frequency modes). The structural analysis methods presented earlier showed good correlation for frequencies and mode shapes in these low-frequency modes. However, during experiments with low-aspect-ratio compressor blades made of composite materials, it was found that flutter can occur at higher frequency modes. In these modes, the largest vibratory motion is usually at the tip. The high frequency vibration leads to high cycle fatigue and loss of the tip of the blade. Analysis methods that predict accurate frequencies and mode shapes at higher modes should be developed.

(7) In order to meet aeroelastic and forced-response constraints, blades of large jet engine fan rotors are often stiffened by one or more sets of part-span shrouds. A major unresolved problem in the dynamic analysis of shrouded rotors is the determination of the appropriate boundary conditions at the blade-shroud interfaces. Nonlinearities are introduced in both the structural and the damping operators because of the nature of dry friction damping and the dependence of boundary conditions on slip and blade displacements. These nonlinearities can give rise to subcritical instabilities and jump phenomena which have a bearing on flutter predictions. Earlier analysis methods used a linearized approach to treat these nonlinearities. With the development of time domain aeroelastic methods, it is now possible to treat nonlinearities more accurately; this approach should be pursued.

(8) Mechanical damping in turbomachines occurs during rubbing at mating interfaces: shroud, root, blade-to-blade or blade-to-disk dampers. Modeling or characterizing material damping has also been a problem for a long time. More accurate modeling of mechanical and material damping is needed for making better aeroelastic predictions.

(9) System analyses are required for making reliable blade and aeroelastic response predictions. The analyses must include multicomponent coupling, such as blade-disk and disk-rotor interactions and support system flexibilities. Substructuring algorithms can provide the necessary aeroelastic information while maintaining accurate overall system responses.

(10) Propulsion research at NASA Lewis is now focusing on advanced ducted fans and turbines. The ultra-high-bypass (UHB) engine concept with ducted, wide-chord fan blades is an example of such trends in engine design. Existing analyses methods need to be modified for these ducted turbomachinery configurations.

(11) Advanced engines require aeroelastic analysis for multiple blade rows, such as rotor-stator stages and counter-rotating propfans. Aeroelastic methods that account for unsteady aerodynamic interactions and structural coupling for these configurations should be developed.

(12) The higher flight Mach numbers planned for the High-Speed Civil Transport (HSCT) will require that thermal analysis be coupled with aeroelastic analysis. Also, acoustic should be developed. Aeroelastic tailoring methods with flutter and blade strain constraints should also be developed for efficient lightweight propulsion components.

(13) Reduction in computational time is a requirement if the models developed are to be useful for design and optimization applications. Methods that use parallel processing and reduced-order models should be vigorously pursued.

Appendix–Formulation and Procedure for Aeroelastic Stability Analysis of Cascades

For completeness, the aeroelastic formulation in the frequency domain (from ref. 18) is presented for the stability analysis of tuned and mistuned cascades: The procedure for predicing the flutter boundary from these equations is also presented. The typical-section structural model is used as an example in presenting the equations. The extension to more refined structural and aerodynamic models is straightforward.

Aeroelastic Analysis for Mistuned Cascades

The following analysis is presented for a generally mistuned cascade in which each blade may have different structural properties. The analysis for the special case of a tuned cascade in which all blades are identical is presented in the subsequent section. The approach followed assumes that the structure is vibrating in an aeroelastic mode (interblade phase angle mode) with a motion that is a harmonic function of time. The frequency of oscillation is permitted to take on complex values, thus allowing decaying-, growing-, or constant-amplitude oscillations. The aerodynamic forces corresponding to constant-amplitude harmonic oscillations are inserted in the equations of motion to formulate a complex eigenvalue problem. The eigenvalues are generally complex quantities, and therefore a complex frequency is obtained. The imaginary part of the complex frequency represents the damping ratio and thus its sign determines whether the motion is decaying or growing; the real part represents the damped frequency of oscillation.

The equations of motion for the typical section (eqs. (9a) and (9b)) with structural damping can be written in matrix form for the s^{th} blade as

$$[M_s]\{\ddot{q}_s\} + [C_s]\{\dot{q}_s\} + [K_s]\{q_s\} = \{f_s\} = \left\{f_{as}^{q}\right\} + \{f_{as}\} \qquad (14)$$

or

$$\begin{bmatrix} 1 & x_{\alpha s} \\ x_{\alpha s} & r_{\alpha s}^2 \end{bmatrix}\begin{Bmatrix} \ddot{h}_s/b \\ \ddot{\alpha}_s \end{Bmatrix} + \begin{bmatrix} 2\omega_{hs}\zeta_{hs} & 0 \\ 0 & 2r_{\alpha s}^2\omega_{\alpha s}\zeta_{\alpha s} \end{bmatrix}\begin{Bmatrix} \dot{h}_s/b \\ \dot{\alpha}_s \end{Bmatrix} + \begin{bmatrix} \omega_{hs}^2 & 0 \\ 0 & r_{\alpha s}^2\omega_{\alpha s}^2 \end{bmatrix}\begin{Bmatrix} h_s/b \\ \alpha_s \end{Bmatrix} = \begin{Bmatrix} f_{hs}/m_s b \\ f_{\alpha s}/m_s b^2 \end{Bmatrix}$$

where $x_\alpha = S_\alpha/mb$ is the distance between the elastic axis and center of mass in semichord units; $r_\alpha = (I_\alpha/mb^2)^{1/2}$ is the radius of gyration about the elastic axis in semichord units; ζ_h and ζ_α are the damping ratios; b is the airfoil semichord; α_s is the pitching displacement; $\omega_h = (K_h/m)^{1/2}$ is the uncoupled natural frequency for bending; $\omega_\alpha = (K_\alpha/I_\alpha)^{1/2}$ is the uncoupled natural frequency for torsion; f_h and f_α are the aerodynamic loads and s varies between 0 and N-1.

It is assumed that the motion of the blades is harmonic in time with a frequency ω and is given by

$$\begin{Bmatrix} h_s/b \\ \alpha_s \end{Bmatrix} = \begin{Bmatrix} h_{os}/b \\ \alpha_{os} \end{Bmatrix} e^{i\omega t} = \sum_{r=0}^{N-1} \begin{Bmatrix} h_{ar}/b \\ \alpha_{ar} \end{Bmatrix} e^{i\omega t} e^{i\sigma_r s} \qquad (15)$$

Note that the motion has been represented as the sum of contributions from each interblade phase angle mode in which each blade has an amplitude h_{ar}/b, α_{ar}, and the phase angle between adjacent blades is

$$\sigma_r = 2\pi r / N \qquad r = 0, 1, 2, \cdots, N-1 \qquad (16)$$

The corresponding aerodynamic forces can be written in terms of the complex-valued unsteady aerodynamic coefficients l_{hh}, $l_{\alpha h}$, $l_{h\alpha}$, $l_{\alpha\alpha}$, l_{wh}, and $l_{w\alpha}$:

$$\begin{Bmatrix} f_{hs}/m_s b \\ f_{\alpha s}/m_s b^2 \end{Bmatrix} = \frac{\omega^2}{\mu_s} \sum_{r=0}^{N-1} \begin{Bmatrix} [l_{hhr} h_{ar}/b + l_{h\alpha r}\alpha_{ar}] \\ [l_{\alpha hr} h_{ar}/b + l_{\alpha\alpha r}\alpha_{ar}] \end{Bmatrix} e^{i\omega t} e^{i\sigma_r s} + \frac{\omega^2}{\mu_s} \sum_{r=0}^{N-1} \begin{Bmatrix} l_{whr} \\ l_{w\alpha r} \end{Bmatrix} e^{i\omega t} e^{i\sigma_r s}$$

where $\mu_s = m_s/\pi\rho_\infty b^2$ is the mass ratio of the blade. Thus, the equations for the s^{th} blade are

$$-\omega^2\begin{bmatrix} 1 & x_{\alpha s} \\ x_{\alpha s} & r_{\alpha s}^2 \end{bmatrix}\begin{Bmatrix} h_{os}/b \\ \alpha_{os} \end{Bmatrix}e^{i\omega t} + i\omega\begin{bmatrix} 2\omega_{hs}\zeta_{hs} & 0 \\ 0 & 2r_{\alpha s}^2\omega_{\alpha s}\zeta_{\alpha s} \end{bmatrix}$$

$$\times \begin{Bmatrix} h_{os}/b \\ \alpha_{os} \end{Bmatrix}e^{i\omega t} + \begin{bmatrix} \omega_{hs}^2 & 0 \\ 0 & r_{\alpha s}^2\omega_{\alpha s}^2 \end{bmatrix}\begin{Bmatrix} h_{os}/b \\ \alpha_{os} \end{Bmatrix}e^{i\omega t}$$

$$= \frac{\omega^2}{\mu_s}\sum_{r=0}^{N-1}\begin{Bmatrix} [l_{hhr}h_{ar}/b + l_{h\alpha r}\alpha_{ar}]e^{i\sigma_r s} \\ [l_{\alpha hr}h_{ar}/b + l_{\alpha\alpha r}\alpha_{ar}]e^{i\sigma_r s} \end{Bmatrix}e^{i\omega t}$$

$$+ \frac{\omega^2}{\mu_s}\sum_{r=0}^{N-1}\begin{Bmatrix} l_{whr} \\ l_{w\alpha r} \end{Bmatrix}e^{i\omega t}e^{i\sigma_r s} \qquad (17)$$

To obtain the eigenvalue problem in the standard form, the damping terms are approximated as

$$2i\omega\omega_{hs}\zeta_{hs} \approx 2i\omega_{hs}^2\zeta_{hs}$$

$$2ir_{\alpha s}^2\omega\omega_{\alpha s}\zeta_{\alpha s} \approx 2ir_{\alpha s}^2\omega_{\alpha s}^2\zeta_{\alpha s}$$

Thus,

$$-\omega^2\begin{bmatrix} 1 & x_{\alpha s} \\ x_{\alpha s} & r_{\alpha s}^2 \end{bmatrix}\begin{Bmatrix} h_{os}/b \\ \alpha_{os} \end{Bmatrix}e^{i\omega t}$$

$$+ \begin{bmatrix} \omega_{hs}^2(1+2i\zeta_{hs}) & 0 \\ 0 & r_{\alpha s}^2\omega_{\alpha s}^2(1+2i\zeta_{\alpha s}) \end{bmatrix}\begin{Bmatrix} h_{os}/b \\ \alpha_{os} \end{Bmatrix}e^{i\omega t}$$

$$= \frac{\omega^2}{\mu_s}\sum_{r=0}^{N-1}\begin{Bmatrix} [l_{hhr}h_{ar}/b + l_{h\alpha r}\alpha_{ar}]e^{i\sigma_r s} \\ [l_{\alpha hr}h_{ar}/b + l_{\alpha\alpha r}\alpha_{ar}]e^{i\sigma_r s} \end{Bmatrix}e^{i\omega t}$$

$$+ \frac{\omega^2}{\mu_s}\sum_{r=0}^{N-1}\begin{Bmatrix} [l_{whr}]e^{i\sigma_r s} \\ [l_{w\alpha r}]e^{i\sigma_r s} \end{Bmatrix}e^{i\omega t} \qquad (18)$$

Rearranging gives

$$-[M_s]\begin{Bmatrix} h_{os}/b \\ \alpha_{os} \end{Bmatrix}e^{i\omega t} + \lambda[K_s]\begin{Bmatrix} h_{os}/b \\ \alpha_{os} \end{Bmatrix}e^{i\omega t}$$

$$= \sum_{r=0}^{N-1}[A_r]\begin{Bmatrix} h_{ar}/b \\ \alpha_{ar} \end{Bmatrix}e^{i\sigma_r s}e^{i\omega t}$$

$$+ \sum_{r=0}^{N-1}\{AD_r\}e^{i\sigma_r s}e^{i\omega t} \qquad (19)$$

where

$$-[M_s] = \mu_s\begin{bmatrix} 1 & x_\alpha \\ x_\alpha & r_\alpha^2 \end{bmatrix}$$

$$[K_s] = \begin{bmatrix} (\omega_{hs}/\omega_o)^2(1+2i\zeta_{hs}) & 0 \\ 0 & r_{\alpha s}^2(\omega_{\alpha s}/\omega_o)^2(1+2i\zeta_{\alpha s}) \end{bmatrix}$$

$$[A_r] = \begin{bmatrix} \ell_{hhr} & \ell_{h\alpha r} \\ \ell_{h\alpha r} & \ell_{\alpha\alpha r} \end{bmatrix} \qquad \{AD_r\} = \begin{Bmatrix} \ell_{whr} \\ \ell_{w\alpha r} \end{Bmatrix} \qquad \lambda = (\omega_o/\omega)^2$$

and ω_o = reference frequency.

To proceed further, the equations for all the N blades on the disk must be considered. For the assumed harmonic blade motion, write

$$\{X\}e^{i\omega t} = [E]\{Y\}e^{i\omega t} \qquad (20)$$

where

$$[E] = \begin{bmatrix} E(0,0)[I] & E(0,1)[I] & \cdots \\ E(1,0)[I] & \ddots & \\ \vdots & & E(N-1,N-1)[I] \end{bmatrix}$$

$$\{X\} = \begin{Bmatrix} h_{o0}/b \\ \alpha_{o0} \\ h_{o1}/b \\ \alpha_{o1} \\ \vdots \\ h_{oN-1}/b \\ \alpha_{oN-1} \end{Bmatrix} \qquad \{Y\} = \begin{Bmatrix} h_{a0}/b \\ \alpha_{a0} \\ h_{a1}/b \\ \alpha_{a1} \\ \vdots \\ h_{aN-1}/b \\ \alpha_{aN-1} \end{Bmatrix}$$

and $E(s,r) = e^{2\pi sri/N}$

Using this relation, we obtain

$$-[E]^{-1}[M][E]\{Y\} + \lambda\,[E]^{-1}[K][E]\{Y\} = [A]\{Y\} + \{AD\} \qquad (21)$$

where

$$[M] = \begin{bmatrix} [M_0] & & & \\ & [M_1] & & \\ & & \ddots & \\ & & & [M_{N-1}] \end{bmatrix}$$

$$[K] = \begin{bmatrix} [K_0] & & & \\ & [K_1] & & \\ & & \ddots & \\ & & & [K_{N-1}] \end{bmatrix}$$

$$[A] = \begin{bmatrix} [A_0] & & & \\ & [A_1] & & \\ & & \ddots & \\ & & & [A_{N-1}] \end{bmatrix}$$

Finally, after rearranging, the equations can be written as

$$[[P] - \lambda[Q]]\{Y\} = -\{AD\} \qquad (22)$$

where

$$[P] = \left[[E]^{-1}[M][E] + [A]\right]$$

$$[Q] = [E]^{-1}[K][E]$$

and

$$\{AD\} = \begin{Bmatrix} AD_0 \\ AD_1 \\ \vdots \\ AD_{N-1} \end{Bmatrix}$$

For a stability calculation (flutter), the motion-independent forces are set to zero, and the eigenvalue problem is obtained in the standard form:

$$[[P] - \lambda[Q]]\{Y\} = \{0\} \qquad (23)$$

The solution of the eigenvalue problem (23) results in 2N complex eigenvalues of the form

$$i\frac{\omega}{\omega_o} = \frac{i}{\sqrt{\lambda}} = \bar{\mu} + i\bar{\nu} \qquad (24)$$

The real part of the eigenvalue $\bar{\mu}$ represents the damping-ratio, and the imaginary part represents the damped frequency; flutter occurs if $\bar{\mu} \geq 0$ for any of the eigenvalues.

The blade aeroelastic response induced by wakes is calculated from equation (22) as

$$\{Y\} = -[[P] - \lambda[Q]]^{-1}\{AD\} \qquad (25)$$

The amplitude of each blade is obtained by substituting equation (25) into equation (20).

Aeroelastic Analysis for a Tuned Cascade

For a tuned cascade (or rotor) in which all the blades are identical, the foregoing analysis can be simplified considerably. In this case, the aeroelastic modes consist of individual blades vibrating with equal amplitudes with a fixed interblade phase angle between adjacent blades. Hence, for this problem, the motion of the typical blade is written as

$$\begin{Bmatrix} h_s/b \\ \alpha_s \end{Bmatrix} = \begin{Bmatrix} h_{os}/b \\ \alpha_{os} \end{Bmatrix} e^{i\omega t} = \begin{Bmatrix} h_{ar}/b \\ \alpha_{ar} \end{Bmatrix} e^{i\omega t} e^{i\sigma_r s} \qquad (26)$$

Thus, the equation for the blade becomes

$$-[M_s]\begin{Bmatrix} h_{ar}/b \\ \alpha_{ar} \end{Bmatrix} e^{i(\omega t+\sigma_r s)} + \lambda\,[K_s]\begin{Bmatrix} h_{ar}/b \\ \alpha_{ar} \end{Bmatrix} e^{i(\omega t+\sigma_r s)}$$

$$= [A_r]\begin{Bmatrix} h_{ar}/b \\ \alpha_{ar} \end{Bmatrix} e^{i(\omega t+\sigma_r s)} + \{AD_r\} e^{i(\omega t+\sigma_r s)} \quad (27)$$

Since the blades are identical, the same equation is obtained for each blade. Thus, no additional information can be obtained by assembling the equations for all the blades on the disk as was done for the general mistuned system. Instead, equation (27) is solved for N different values of the interblade phase angle given by equation (16). As before, the equations for the forced-response problem are obtained by setting the motion-dependent forces to zero; the equations for the flutter problem are obtained by setting the motion-independent forces to zero.

For the stability calculation, the equation can be simplified as

$$\left([P_r] - \lambda[I]\right)\{Y\} = \{0\} \quad (28)$$

where

$$[P_r] = \begin{bmatrix} \dfrac{\mu + l_{hhr}}{\mu(\omega_h/\omega_\alpha)^2(1+2i\zeta_h)} & \dfrac{\mu x_\alpha + l_{h\alpha r}}{\mu(\omega_h/\omega_\alpha)^2(1+2i\zeta_h)} \\ \dfrac{\mu x_\alpha + l_{h\alpha r}}{\mu r_\alpha^2(1+2i\zeta_\alpha)} & \dfrac{\mu r_\alpha^2 + l_{\alpha\alpha r}}{\mu r_\alpha^2(1+2i\zeta_\alpha)} \end{bmatrix}$$

where the subscript s identifying the blade has been dropped and the reference frequency ω_0 has been chosen to be equal to the torsional frequency ω_α.

The solution of the foregoing eigenvalue problem results in two complex eigenvalues of the form $\bar{\mu} + i\bar{\nu}$ (as discussed in Aeroelastic Analysis for Mistuned Cascades), and flutter occurs if $\bar{\mu} \geq 0$. For the tuned rotor, the stability of each phase angle mode is examined separately. Hence, the interblade phase angle is fixed at one of the values given by equation (16), and the 2×2 eigenvalue problem is solved. The value of the interblade phase angle is then changed, and the procedure is repeated for each of the N permissible values. The critical phase angle is identified as the one which results in the lowest flutter speed.

Stability Calculation

The aerodynamic coefficients are calculated before the eigenvalue problem can be set up and solved. Since the unsteady aerodynamic coefficients depend on the frequency of oscillation, it is necessary to assume a frequency ω (reduced frequency of blade vibration k_c) in advance to be able to calculate the aerodynamic coefficients. In actual calculations, the aerodynamic coefficients are functions of the inlet Mach number M_∞, and the interblade phase angle σ_r, in addition to cascade geometric parameters. Either of the following two procedures can be used in flutter calculations. In the first procedure, a value of the inlet Mach number is assumed, and the reduced frequency is varied until the real part of one of the eigenvalues $\bar{\mu}$ becomes zero while the real parts of the remaining eigenvalues are negative. The assumed flutter-reduced frequency k_{cf} and the calculated flutter frequency $\bar{\nu}_f$ are both based on ω_f. Thus, these two can be combined to eliminate ω_f, and the flutter speed is obtained, namely, $V_f = \bar{\nu}_f c\ \omega_f/k_{cf}$. Since the inlet Mach number is assumed to be known, this flutter speed gives the inlet condition (speed of sound a_∞) at which the rotor will be neutrally stable at the assumed Mach number. The first procedure can be repeated to obtain a plot of flutter speed versus Mach number. Knowing the operating conditions, it is possible to determine whether flutter will occur within the operating region and if so, the Mach number and frequency at flutter. In the second procedure, the inlet conditions (M_∞ and a_∞) are assumed to be known. A value of reduced frequency is assumed and the eigenvalue problem is solved. The values of frequency ω calculated from the reduced frequency k_c and from the imaginary part of the eigenvalue $\bar{\nu}$ are compared. If they do not agree, a new value of reduced frequency is assumed and the calculations repeated until the frequencies match. The sign of the real part of the eigenvalue $\bar{\mu}$ is then used to decide if flutter will occur. It should be noted that the analysis of a mistuned cascade requires the solution of the equations for all phase angles at one time for a given reduced frequency. This is very time consuming; a procedure is being developed to reduce this time (ref. 66).

Acknowledgments

This work is supported by NASA grants NAG3–1137, NAG3–1234, and NAG3–1230. The authors would like to acknowledge G.V. Brown, A. Kurkov, D.L. Hoyniak, and C. Lawrence for their suggestions on the future directions.

Lewis Research Center
National Aeronautics and Space Administration
Cleveland, Ohio
March 8, 1993

References

1. Ball, C.L.: Advanced Technologies Impact on Compressor Design and Development: A perspective. NASA TM–102341, 1989.
2. Jeffers, J.D., II; and Meece, C.E., Jr.: F100 Fan Stall Flutter Problem Review and Solution. J. Aircr., vol. 12, Apr. 1975, pp. 350–357.
3. Mikolajczak, A.A., et al.: Advances in Fan and Compressor Blade Flutter Analysis and Predictions. J. Aircr., vol. 12, Apr. 1975, pp. 325–332.
4. Lubomski, J.F.: Status of NASA Full-Scale Engine Aeroelasticity Research. AIAA/ASME/ASCE/AHS/ASC Structures, Structural Dynamics, and Materials Conference, 21st, AIAA, New York, 1980, p. 18 (Also, NASA TM–81500, 1980.)
5. Mehmed, O., et al.: Bending-Torsion Flutter of a Highly Swept Advanced Turboprop. NASA TM–82975, 1981.
6. Mehmed, O.; and Kaza, K.R.V.: Experimental Classical Flutter Results of a Composite Advanced Turboprop Model. NASA TM–88792, 1986.
7. Guruswamy, G.P.: Interaction of Fluids and Structures for Aircraft Applications. Comput. Struct., vol. 30, no. 1/2, 1988, pp. 1–13.
8. Edwards, J.W.; and Thomas, J.L.: Computational Methods for Unsteady Transonic Flows. Unsteady Transonic Aerodynamics, D. Nixon, ed., Progress in Astronautics and Aeronautics, Vol. 120, AIAA, Washington, DC, pp. 211–261, 1989. (Also, NASA TM–89106, 1987).
9. Platzer, M.F.; and Carta, F.O., eds.: Aeroelasticity in Axial-Flow Turbomachines. Vol. 1: Unsteady Turbomachinery Aerodynamics. AGARD AG–298–VOL–1, 1987.
10. Platzer, M.F.; and Carta, F.L., eds.: Aeroelasticity in Axial-Flow Turbomachines. Vol. 2: Structural Dynamics and Aeroelasticity. AGARD AG–298–VOL–2, 1987.
11. Bendiksen, O.O.: Aeroelastic Problems in Turbomachines. AIAA/ASME/ASCE/AHS/ASC Structures, Structural Dynamics and Materials Conference, 31st, AIAA, New York, 1990, pp. 1736–1761.
12. Claus, R.W.; Evans, A.L.; and Follen, G.: Multidisciplinary Propulsion Simulation Using NPSS. AIAA Paper 92–4709, 1992.
13. Kaza, K.R.V.: Development of Aeroelastic Analysis Methods for Turborotors and Propfans-Including Mistuning. Lewis Structures Technology, 1988, Vol.1: Structural Dynamics, NASA CP–3003–VOL–1, 1988, pp. 247–262.
14. Hoyniak, D.; and Fleeter, S.: The Effect of Circumferential Aerodynamic Detuning on Coupled Bending-Torsion Unstalled Supersonic Flutter. J. Turbomach., vol. 108, Oct. 1986, pp. 253–260.
15. Crawley, E.F.: Aeroelastic Formulations for Turbomachines and Propellers. Aeroelasticity in Axial-Flow Turbomachines, Vol. 1: Unsteady Turbomachinery Aerodynamics. M.F. Platzer and F.O. Carta, eds., AGARD AG–298–VOL–1, 1987, Paper No. 19, pp. 19– 1–19–24.
16. Bathe, K.J.; and Wilson, E.L.: Numerical Methods in Finite Element Analysis. Prentice-Hall, EnglewoodCliffs, NJ, 1976.
17. Lane, F.: System Mode Shapes in the Flutter of Compressor Blade Rows. J. Aeronaut. Sci., vol. 23, no.1, 1956, pp. 54–66.
18. Kaza, K.R.V.; and Kielb, R.E.: Flutter and Response of a Mistuned Cascade in Incompressible Flow. AIAA J., vol. 20, no. 8, 1982, pp. 1120–1127.
19. Kaza, K.R.V.; and Kielb, R.E.: Flutter of Turbofan Rotors with Mistuned Blades. AIAA J., vol. 22, no.11, 1984, pp. 1618–1625.
20. Kaza, K.R.V.; and Kielb, R.E.: Vibration and Flutter of Mistuned Bladed-Disk Assemblies. J. Propul. Power, vol. 1, no. 5, 1985, pp. 336–344.
21. Kaza, K.R.V., et al.: Analytical Flutter Investigation of a Composite Propfan Model. J. Aircr., vol. 26, no. 8, Aug. 1989, pp. 772–780.
22. McGee, O.G.: Finite Element Analysis of Flexible, Rotating Blades. NASA TM–89906, 1987.
23. Lawrence, C., et al.: A NASTRAN Primer for the Analysis of Rotating Flexible Blades. NASA TM–89861, 1987.
24. Huff, D.L.; Swafford, T.W.; and Reddy, T.S.R.: Euler Flow Predictions for an Oscillating Cascade Using a High Resolution Wave-Split Scheme. ASME Paper 91–GT–198, 1991. (Also, NASA TM–104377, 1991.)
25. Srivastava, R.: An Efficient Hybrid Scheme for the Solution of Rotational Flow Around Advanced Propellers. Ph.D. Thesis, Georgia Institute of Technology, Atlanta, GA, 1990.
26. Kao, Y.F.: A Two-Dimensional Unsteady Analysis for Transonic and Supersonic Cascade Flows. Ph.D. Thesis, School of Aeronautics and Astronautics, Purdue University, West Lafayette, IN, 1989.
27. Ku, C.C.; and Williams, M.H.: Three Dimensional Full Potential Method for the Aeroelastic Modeling of Propfans. AIAA Paper 90–1120, 1990.
28. Verdon, J.M.; and Caspar, J.R.: A Linearized Unsteady Aerodynamic Analysis for Transonic Cascades. J. Fluid Mech., vol. 149, 1984, pp. 403–429.
29. Hall, K.C.; and Clark, W.S.: Prediction of Unsteady Aerodynamic Loads in Cascades Using the Linearized Euler Equations on Deforming Grids. AIAA Paper 91–3378, 1991.
30. Whitehead, D.S.: Force and Moment Coefficients for Vibrating Aerofoils in Cascade. Report ARC–R&M–3254, Aeronautical Research Council, London, England, 1960.
31. Smith, S.N.: Discrete Frequency Sound Generation in Axial Flow Turbomachines. Report ARC–R&M–3709, Aeronautical Research Council, London, England, 1960.
32. Rao, B.M.; and Jones, W.P.: Unsteady Airloads on a Cascade of Staggered Blades in Subsonic Flow. Paper No. 32, Unsteady Pheno-mena in Turbomachinery, AGARD CP–177, 1975.
33. Goldstein, M.E.; Braun, W.; and Adamczyk, J.J.: Unsteady Flow in a Supersonic Cascade with Strong In-Passage Shocks. J. Fluid Mech., vol. 83, Pt. 3, 1977, pp. 569–604.
34. Adamczyk, J.J.; and Goldstein, M.E.: Unsteady Flow in a Supersonic Cascade with Subsonic Leading Edge Locus. AIAA J., vol. 16, no. 12, Dec. 1978, pp. 1248–1254.
35. Surampudi, S.P.; and Adamczyk, J.J.: Unsteady Transonic Flow Over Cascade Blades. AIAA J., vol. 24, no. 2, Feb. 1986, pp. 293–302.
36. Lane, F.: Supersonic Flow Past an Oscillating Cascade with Supersonic Leading-Edge Locus. J. Aeronaut. Sci., vol. 24, no. 1, Mechanical Engineering, University of Toledo, Toledo, OH, 1991.
37. Bakhle, M.A., et al.: Cascade Flutter Analysis with Transient Response Aerodynamics. Comput. Struct., vol. 41, no. 5, 1991, pp. 1073–1085.
38. Janetzke, D.C.; and Murthy, D.V.: Concurrent Processing Adaptation of Aeroelastic Analysis of Propfans. NASA TM–102455, 1990.
39. Mahajan, A.J.; Bakhle, M.A.; and Dowell, E.H.: An Efficient Procedure for Cascade Aeroelastic Stability Determination Using Nonlinear, Time-Marching Solvers. AIAA Paper 93–1631, 1993.
40. Adamczyk, J.J.: Analysis of Supersonic Stall Bending Flutter in Axial-Flow Compressor by Actuator Disk Theory, NASA TP–1345, 1978.
41. Reddy, T.S.R.; and Mehmed, O.: Aeroelastic Analysis of Prop Fan Blades with a Semi-Empirical Dynamic Stall Model. AIAA Paper 89–2695, 1989. (Also NASA TM–4083, 1989.)
42. Kielb, R.E.; and Ramsey, J.K.: Flutter of a Fan Blade in Supersonic Axial Flow. J. Turbomach., vol. 111, no. 10, Oct. 1989, pp. 462–467.
43. Williams, M.H.: An Unsteady Lifting Surface Method for Single Rotation Propellers. NASA CR–4302, 1990.
44. Williams, M.H.; Cho, J.; and Dalton, W.N.: Unsteady Aerodynamic Analysis of Ducted Fans. J. Propul. Power, vol. 7, no. 5, 1990, pp. 800–804.
45. Adamczyk, J.J.; Goldstein, M.E.; and Hartman, M.J.: Supersonic Unstalled Flutter. Stresses, Vibrations, Structural Integration and Engine Integrity, AGARD CP–248, 1978, pp. 35-1–35-14.

46. Kielb, R.E.; and Kaza, K.R.V.: Aeroelastic Characteristics of a Cascade of Mistuned Blades in Subsonic and Supersonic Flows. J. Vibr. Acoust. Stress Reliab. Design, vol. 105, Oct. 1983, pp. 425–433.
47. Busbey, B.C.; Kaza, K.R.V.; and Keith, T.G., Jr.: The Effects of Strong Shock Loading on Coupled Bending-Torsion Flutter of Tuned and Mistuned Cascades. Fluid-Structure Interaction and Aerodynamic Damping; Proceedings of the Tenth Biennial Conference on Mechanical Vibration and Noise, E.H. Dowell and M.K. Young, eds., ASME, New York, 1985, pp. 93–108.
48. Mahajan, A., et al.: Aeroelastic Stability Analyses of Two Counter Rotating Propfan Designs for Cruise Missile Model. NASA TM–105268, 1992.
49. Elchuri, V.; and Smith, G.C.C.: Flutter Analysis of Advanced Turbopropellers. Structural Dynamics and Materials Conference, 24th pt. 2, AIAA, New York, 1985, pp. 160–165. (Also, AIAA Paper 83–0846, 1983.)
50. Kaza, K.R.V., et al.: Analytical and Experimental Investigation of Mistuning in Propfan Flutter. NASA TM–88959, 1987.
51. August, R.; and Kaza, K.R.V.: Vibration, Performance, Flutter and Forced Response Characteristics of a Large-Scale Propfan and Its Aeroelastic Model. AIAA Paper 88–3155, 1988. (Also NASA TM–101322, 1988.)
52. Kaza, K.R.V., et al.: Aeroelastic Response of Metallic and Composite Propfan Models in Yawed Flow, AIAA Paper 88–3154, 1988. (Also NASA TM–100964, 1988.)
53. Smith, T.E.; and Kadambi, J.R.: The Effect of Steady Aerodynamic Loading on the Flutter Stability of Turbomachinery Blading. ASME Paper 91–GT–130, 1991.
54. Smith, T.E.: A Model Aeroelastic Analysis Scheme for Turbomachinery Blading. NASA CR–187089, 1991.
55. Pierre, C.; Smith,T.E.; and Murthy, D.V.: Localization of Aeroelastic Modes in Mistuned High-Energy Turbines. AIAA Paper 91–3379, 1991.
56. Murthy, D.V.; and Stefko, G.L.: FREPS–A Forced Response Prediction System for Turbomachinery Blade Rows. AIAA Paper 92–3072, 1992.
57. Bakhle, M.A.; Keith, T.G. Jr.; and Kaza, K.R.V.: Application of a Full Potential Solver to Bending-Torsion Flutter in Cascades. AIAA Paper 89–1386, 1989.
58. Bakhle, M.A.; Reddy, T.S.R.; and Keith, T.G., Jr.: Time Domain Flutter Analysis of Cascades Using a Full Potential Solver. AIAA J., vol. 30, no. 1, Jan 1992, pp. 163–170.
59. Bakhle, M.A.; Reddy, T.S.R.; and Keith, T.G., Jr.: An Investigation of Cascade Flutter Using Two Dimensional Full Potential Solver. AIAA Paper 92–2119, 1992.
60. Bakhle, M.A.: Flutter Analysis of Cascades Based on the Two Dimensional Full Potential Equation. Ph.D. Thesis, Department of Mechanical Engineering, University of Toledo, Toledo, OH, 1991.
61. Isogai, K.: Numerical Study of Transonic Flutter of a Two Dimensional Airfoil. Report NAL–TR–617T, National Aerospace Laboratory, Tokyo, Japan, 1980.
62. Reddy, T.S.R., et al.: Flutter Analysis of Cascades Using a Two-Dimensional Euler Solver. AIAA Paper 91–1681, 1991.
63. Reddy, T.S.R., et al.: Analysis of Cascades Using a Two-Dimensional Euler Aeroelastic Solver. AIAA Paper 92–2370, 1992.
64. Srivastava, R., et al.: Application of an Efficient Hybrid Scheme for Aeroelastic Analysis of Advanced Propellers. J. Propul. Power, vol. 7, no. 5, 1991, pp. 767–775.
65. Srivastava, R.; and Mehmed, O.: On The Static Stability of Forward Swept Propfans. AIAA Paper 93–1634, 1993.
66. Murthy, D.V.; and Pierre, C.: An Efficient Constraint to Account for Mistuning Effects in the Optimal Design of Engine Rotors. AIAA Paper 92–4711, 1992.

REPORT DOCUMENTATION PAGE

Form Approved
OMB No. 0704-0188

1. AGENCY USE ONLY (*Leave blank*)	2. REPORT DATE	3. REPORT TYPE AND DATES COVERED
	September 1993	Technical Paper

4. TITLE AND SUBTITLE

A Review of Recent Aeroelastic Analysis Methods for Propulsion at NASA Lewis Research Center

5. FUNDING NUMBERS

WU-535-03-01/505-63-5B

6. AUTHOR(S)

T.S.R. Reddy, Milind A. Bakhle, R. Srivastava, Oral Mehmed, and George L. Stefko

7. PERFORMING ORGANIZATION NAME(S) AND ADDRESS(ES)

National Aeronautics and Space Administration
Lewis Research Center
Cleveland, Ohio 44135-3191

8. PERFORMING ORGANIZATION REPORT NUMBER

E-7535

9. SPONSORING/MONITORING AGENCY NAME(S) AND ADDRESS(ES)

National Aeronautics and Space Administration
Washington, D.C. 20546-0001

10. SPONSORING/MONITORING AGENCY REPORT NUMBER

NASA TP-3406

11. SUPPLEMENTARY NOTES

T.S.R. Reddy, Milind A. Bakhle, R. Srivastava, University of Toledo, Toledo, Ohio 43606. Oral Mehmed and George L. Stefko, NASA Lewis Research Center. Responsible person, George L. Stefko, (216) 433-3920.

12a. DISTRIBUTION/AVAILABILITY STATEMENT

Unclassified - Unlimited
Subject Category 39

12b. DISTRIBUTION CODE

13. ABSTRACT (*Maximum 200 words*)

This report reviews aeroelastic analyses for propulsion components (propfans, compressors and turbines) being developed and used at NASA Lewis Research Center. These aeroelastic analyses include both structural and aerodynamic models. The structural models include a typical section, a beam (with and without disk flexibility), and a finite-element blade model (with plate bending elements). The aerodynamic models are based on the solution of equations ranging from the two-dimensional linear potential equation to the three-dimensional Euler equations for multibladed configurations. Typical calculated results are presented for each aeroelastic model. Suggestions for further research are made. Many of the currently available aeroelastic models and analysis methods are being incorporated in a unified computer program, APPLE (Aeroelasticity Program for Propulsion at LEwis).

14. SUBJECT TERMS

Turbomachines; Propfans; Cascades; Aeroelasticity; Neural networks; Computer software; Optics

15. NUMBER OF PAGES

26

16. PRICE CODE

A03

17. SECURITY CLASSIFICATION OF REPORT	18. SECURITY CLASSIFICATION OF THIS PAGE	19. SECURITY CLASSIFICATION OF ABSTRACT	20. LIMITATION OF ABSTRACT
Unclassified	Unclassified	Unclassified	